

## **A review of structural inheritance in rift basin formation**

Anindita Samsu<sup>1</sup>, Steven Micklethwaite<sup>2</sup>, Jack N. Williams<sup>3</sup>, Åke Fagereng<sup>4</sup>, Alexander R. Cruden<sup>1</sup>

<sup>1</sup>*School of Earth, Atmosphere and Environment, Monash University, Melbourne, Australia*

<sup>2</sup>*Sustainable Minerals Institute, University of Queensland, Brisbane, Australia*

<sup>3</sup>*Department of Geology, University of Otago, Dunedin, New Zealand*

<sup>4</sup>*School of Earth and Environmental Sciences, Cardiff University, Cardiff, UK*

[anindita.samsu@monash.edu](mailto:anindita.samsu@monash.edu)

@anungsamsu

[S.Micklethwaite@uq.edu.au](mailto:S.Micklethwaite@uq.edu.au)

@EarthSkyOcean1

[jack.williams@otago.ac.nz](mailto:jack.williams@otago.ac.nz)

@faulty\_Jack

[fagerenga@cardiff.ac.uk](mailto:fagerenga@cardiff.ac.uk)

@akefagereng

[sandy.cruden@monash.edu](mailto:sandy.cruden@monash.edu)

@SandyCruden

---

This manuscript is a pre-print and has been submitted for publication in **Earth-Science Reviews**. It is currently undergoing peer-review. Subsequent versions of this manuscript may have slightly different content. If accepted, the final version of this manuscript will be available via the “Peer-reviewed Publication DOI” link on the right hand side of this webpage. Please feel free to contact any of the authors directly; we welcome feedback.

---

1 A review of structural inheritance in rift basin formation

2 Anindita Samsu<sup>1</sup>, Steven Micklethwaite<sup>2</sup>, Jack N. Williams<sup>3</sup>, Åke Fagereng<sup>4</sup>, Alexander R.  
3 Cruden<sup>1</sup>

4 <sup>1</sup>*School of Earth, Atmosphere and Environment, Monash University, Melbourne, Australia*

5 <sup>2</sup>*Sustainable Minerals Institute, University of Queensland, Brisbane, Australia*

6 <sup>3</sup>*Department of Geology, University of Otago, Dunedin, New Zealand*

7 <sup>4</sup>*School of Earth and Environmental Sciences, Cardiff University, Cardiff, UK*

8

9 Keywords: Rifting, rift basin, structural inheritance, reactivation, strain re-orientation, East  
10 African Rift System

11

12 **ABSTRACT**

13 In the context of rift basin formation, structural inheritance describes the influence of pre-existing  
14 basement structures on new, rift-related structures, including faults. Examples of basin features  
15 influenced by inheritance include rift localisation and segmentation at the plate scale, as well as  
16 variations in the geometries, orientations, and kinematics of individual rift-related faults. Given  
17 that continental rifts commonly form in pre-deformed crust, structural inheritance is likely to be  
18 the norm, not the exception. As such, structural inheritance has implications for reconstructing the  
19 paleotectonic history of rifts, investigating seismic hazards, and understanding the fluid transport  
20 and storage capabilities of natural fracture systems in the context of geo-energy and ore deposits.  
21 Our review of the literature shows that inheritance is driven by several mechanisms, which include  
22 frictional reactivation and local re-orientation of the far-field strain and/or stress. Here we highlight

23 how insights from field observations, geophysics, and analogue and numerical models can be used  
24 to classify these mechanisms in terms of hard-linked and soft-linked inheritance. We demonstrate  
25 how different inheritance mechanisms can produce different geometric and kinematic relationships  
26 between pre-existing basement structures and rift-related faults, and that these mechanisms can be  
27 active at different depths within the same rift. Our aim is to provide a framework for recognising  
28 various expressions of structural inheritance and their underlying mechanism(s) in natural rifts, so  
29 that we can better interpret basement structures under cover and are equipped with additional  
30 constraints for understanding the multi-stage evolution of basement-influenced rift basins  
31 worldwide.

## 32 1. INTRODUCTION

33 Continental rifts commonly form in crust with a pre-existing structural framework. Given the  
34 appropriate stress orientations, stress magnitudes, fluid pressures, and thermal gradients of the  
35 crust, these structures exert a control on the development of rifts and rift-related structures (e.g.,  
36 Wilson, 1966; Morley, 1995; Krabbendam and Barr, 2000; Schumacher, 2002; Chenin and  
37 Beaumont, 2013; Fossen et al., 2016; Schiffer et al., 2018, 2020). This **structural inheritance**  
38 operates at multiple scales in both frictional and viscous layers of the crust and influences the  
39 location, geometry, and internal architecture of rift basins (examples in Table 1). Lithospheric-  
40 scale weaknesses up to thousands of kilometres in length span the frictional-viscous transition and  
41 localise and segment entire rift systems (McConnell, 1972; Daly et al., 1989; Versfelt and  
42 Rosendahl, 1989; Wheeler and Karson, 1989; Piqué and Laville, 1996; Doré et al., 1997;  
43 Holdsworth et al., 2001a; Miller et al., 2002; Gibson et al., 2013; Molnar et al., 2017; Peace et al.,  
44 2018b; Heron et al., 2019). They also modulate the evolution of the lithosphere and magmatic  
45 budget during rifting, in some cases up to the continental break-up and passive margin stages (e.g.,  
46 Dunbar and Sawyer, 1989; Buitter and Torsvik, 2014; Petersen and Schiffer, 2016; Gouiza and  
47 Paton, 2019; Gouiza and Naliboff, 2021). In the brittle crust, weaknesses at length scales of tens  
48 of kilometres or less influence the orientations and distributions of basin-bounding and basin-  
49 internal faults, some of which are misoriented with respect to inferred plate motion directions (e.g.,  
50 Morley et al., 2004; Lyon et al., 2007; Wilson et al., 2010).

51 Many studies invoking the influence of pre-rift basement structures on rift-related faults pay  
52 particular attention to frictional **reactivation**, which describes structures that have accommodated  
53 displacement during multiple discrete (i.e., intervals  $>1$  Ma) deformation events (sensu  
54 Holdsworth et al., 1997). These structures include lithological contacts (Ashby, 2013; Holdsworth

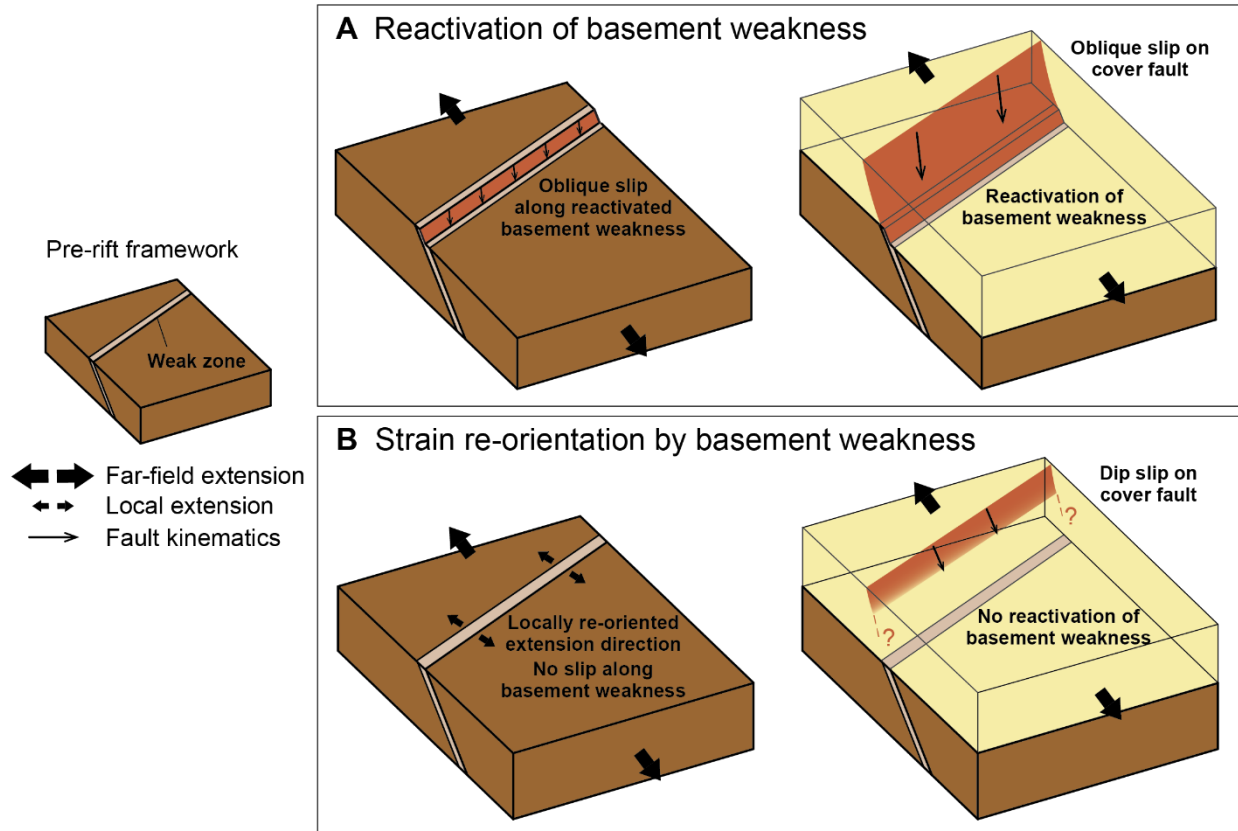
55 et al., 2020; Wedmore et al., 2020a), faults or fault zones (McCaffrey, 1997; Holdsworth et al.,  
56 2001b), older rift fabrics (Whipp et al., 2014; Bladon et al., 2015; Duffy et al., 2015; Deng et al.,  
57 2017a; McHarg et al., 2019; Phillips and McCaffrey, 2019; Wang et al., 2021), and shear zones  
58 and the metamorphic fabrics within them (Kirkpatrick et al., 2013; Bird et al., 2014; Phillips et al.,  
59 2016; Fazlikhani et al., 2017; Kolawole et al., 2018; Peace et al., 2018a; Heilman et al., 2019;  
60 Wedmore et al., 2020b). Such focus on reactivation has resulted in the synonymous use of the  
61 terms *structural inheritance* and *reactivation*; in some cases, the two terms are used  
62 interchangeably (e.g., Corti et al., 2007; Manatschal et al., 2015). This usage is problematic, as it  
63 does not acknowledge other mechanisms by which pre-rift basement structures influence rift-  
64 related deformation. It also suggests that there is limited or no influence of pre-existing structures  
65 in areas where we have no evidence of reactivation (as defined by Holdsworth et al., 1997).

66 A number of field and modelling studies point to subtle mechanisms, such as the re-orientation of  
67 strain (Corti et al., 2013b; Philippon et al., 2015; Hodge et al., 2018; Samsu et al., 2021) and stress  
68 (Bell, 1996; Morley, 2010; Tingay et al., 2010a), through which pre-rift basement structures can  
69 influence deformation localisation and distribution without exhibiting significant (i.e., observable)  
70 signs of repeated slip or displacement on pre-existing structures themselves. It is important to  
71 distinguish between inheritance mechanisms, as they have different implications for the kinematics  
72 of rift-related faults, the interpretation of far-field paleo-extension and paleo-stress directions, and  
73 hard and/or soft linkage between pre-rift basement structures and rift-related faults (Figure 1).

74 In this paper, we explore the multifaceted ways in which heterogeneous basement rocks can control  
75 fault system geometry and influence deformation in the overlying cover rocks during rift basin  
76 formation in magma-poor rifts. In this context, we consider the crust to be rheologically layered  
77 with a thermally controlled transition separating an upper frictional and lower viscous regime

78 (sensu Handy et al., 2007). A more complete picture of different inheritance mechanisms can help  
79 us clarify the mechanical controls on rift and basin evolution and open up opportunities to: (i)  
80 “uncover” the characteristics of buried basement rocks that are commonly poorly imaged in  
81 geophysical surveys; (ii) better understand the structural evolution of rifted margins; and (iii)  
82 provide additional constraints on plate reconstructions. Understanding the potential impact of pre-  
83 existing basement structures on younger fault networks also has implications for seismic hazards  
84 assessment (e.g., Fonseca, 1988; Wedmore et al., 2020b; Hecker et al., 2021), geothermal energy  
85 (e.g., Schumacher, 2002; Bertrand et al., 2018), mineral exploration (e.g., Rowland and Sibson,  
86 2004), and CO<sub>2</sub> and nuclear waste storage (e.g., Barton and Zoback, 1994; Andrés et al., 2016).  
87 In the first part of this review, we synthesise research on structural inheritance during rift basin  
88 formation. We focus on the impact of inheritance on faults that strike obliquely to the inferred far-  
89 field extension direction but formed or are active during rifting. Observations from field and  
90 geophysical data are presented first, followed by insights from analogue and numerical models  
91 and geomechanical theory (Section 2). In the Discussion, we propose two mechanisms that  
92 underpin all instances of structural inheritance, namely reactivation and strain re-orientation  
93 (Section 3.1). We also suggest a classification of observed basement-cover relationships into hard-  
94 linked and soft-linked inheritance and interpret the mechanisms behind them (Section 3.2). Finally,  
95 we apply this framework to a natural rift system (i.e., the East African Rift System; Section 3.3)  
96 and discuss the implications of structural inheritance for natural resources exploration (Section  
97 3.4).

98



99

100 Figure 1 A pre-existing basement weakness, striking obliquely to the far-field extension direction,  
 101 can influence the orientation and kinematics of rift-related faults (e.g., normal faults) in the  
 102 overlying cover. Different inheritance mechanisms can have different impacts on fault kinematics  
 103 and linkage between a rift-related cover fault and basement weakness, despite the two exhibiting  
 104 geometric similarity in map view in both scenarios. Reactivation of the basement weakness (A) is  
 105 commonly associated with oblique slip along the basement weakness and cover fault (e.g., Morley,  
 106 1995; Corti et al., 2007), in addition to hard linkage between the two structures (Phillips et al.,  
 107 2016). A second mechanism through which the basement weakness can influence rift-related  
 108 faulting is local re-orientation of the far-field strain (B), which may result in dip-slip kinematics  
 109 along the cover fault (Philippon et al., 2015).

110 Here we refer to **basement** as any rock underlying the sedimentary **cover**, which we define as  
 111 basin fill related to the current rift-related episode. The basement can comprise multiple units  
 112 overlying one another and may include basin fill from previous rift episodes. While we  
 113 acknowledge that inheritance can impact all kinds of brittle structures (e.g., faults, joints, dykes,  
 114 etc.) during and after rifting, here we focus on the influence of pre-rift (a.k.a. pre-existing)

115 basement structures on rift-related faults. Pre-existing basement structures include discrete  
116 discontinuities (e.g., the contact between a dyke and surrounding host rock; a fault or fault zone;  
117 the boundary between two rheologically distinct terranes), pervasive strength anisotropies (e.g.,  
118 penetrative metamorphic or rift fabrics from previous collisional or extensional events), and  
119 lithospheric-scale weaknesses in the viscous lower crust or lithospheric mantle (Table 1).



120 Table 1 Natural examples of pre-existing basement features, their influence on subsequent deformation in the overlying cover, and the  
 121 resulting geometries which can be observed.

Pre-existing feature	Scale	Mechanism	Observation(s)	Example(s)
<b>Rheological boundary (crustal-scale)</b>				
Dyke-host rock contact		Reactivation	Geometric similarity	Lower Shire Graben, southern Malawi Rift (Wedmore et al., 2020); NW Scotland (Holdsworth et al., 2020)
<b>Discrete fabric</b>				
Fault or cemented fault zone		Reactivation	Geometric similarity	North Sea Rift (Deng et al., 2017a)
		Stress perturbation	Local stress re-orientation	North Sea Rift (Bell, 1996; Yale, 2003)
<b>Pervasive strength</b>				
Metamorphic foliation within shear zone	10s of km	Stress perturbation	3D transtensional strain	North Sea Rift (Reeve et al., 2015; Osagiede et al., 2020); East African Rift (Morley et al., 2010 and references therein)
	10s of km	Reactivation	Geometric similarity	Northern Thailand (Morley et al., 2004); North Sea Rift (Færseth et al., 1995; Phillips et al., 2016; Fazlikhani et al., 2017); offshore New Zealand (Muir et al., 2000; Collanega et al., 2019; Phillips & McCaffrey, 2019); onshore New Zealand (Villamor et al., 2017); East African Rift System (Laó-Dávila et al., 2015; Dawson et al., 2018); East Greenland Rift System (Rotevatn et al., 2018); onshore and offshore Norway (Fossen & Hurich, 2005; Fossen et al., 2014; Fossen et al., 2016)
Rift fabric	10s of km	Reactivation	Non-colinear normal fault sets	Barmer Basin, NW India (Bladon et al., 2015); Horda Platform, North Sea (Whipp et al., 2014; Duffy et al., 2015); Bohai Bay Basin, eastern China (Wang et al., 2021); Great South Basin, offshore New Zealand (Phillips & McCaffrey, 2019); Northern Carnavron Basin, Western Australia (McHarg et al., 2019)
<b>Rheological boundary (lithospheric-scale)</b>				
Terrane boundary	10s of km	Barrier to fault propagation	Fault splay	Great South Basin, offshore New Zealand (Phillips & McCaffrey, 2019); Sudan Rift System (Daly et al., 1989)
<b>Lithospheric weakness</b>				
Orogenic structures, including shear zones (i.e., terrane boundary, suture zone, orogenic belt, mobile belt)	10s–1000s of km	Strain localisation	Rift localisation & segmentation	North Atlantic (Wilson, 1966; Piqué & Laville, 1996; Doré et al., 1997; Buitter & Torsvik, 2014; Petersen & Schiffer, 2016; Schiffer et al., 2018); South Atlantic (Krabbendam & Barr, 2000); East African Rift System (McConnell, 1972; Daly et al., 1989; Versfelt & Rosendahl, 1989; Wheeler & Karson, 1989; Smith and Mosley, 1993; Ring, 1994; Theunissen et al., 1996; Morley, 2010; Kolawole et al., 2018; Muirhead & Kattenhorn, 2018; Wedmore et al., 2020); Gondwana break-up along Pan African mobile belts (Sykes, 1978); Karoo Rift Basins (Daly et al., 1989); Baikal Rift (Petit et al., 1996); West Greenland Rift System (Heron et al., 2019); offshore southern Norway (Færseth et al., 1995; Phillips et al., 2016); onshore New Zealand (Rowland and Sibson, 2004); offshore New Zealand (Muir et al., 2000; Mortimer et al., 2002; Phillips & McCaffrey, 2019); Australian Southern Margin (Miller et al., 2002; Gibson et al., 2013)
Pervasive anisotropic crystalline fabric within lithospheric mantle	10s–1000s of km		Rift localisation	North, Central & South Atlantic (Vauchez et al., 1997; Tommasi & Vauchez, 2001)

122

## 123 2. EXAMPLES AND INSIGHTS FROM NATURE AND MODELS

### 124 2.1. Observations of basement-cover interactions from geophysical data and outcrops

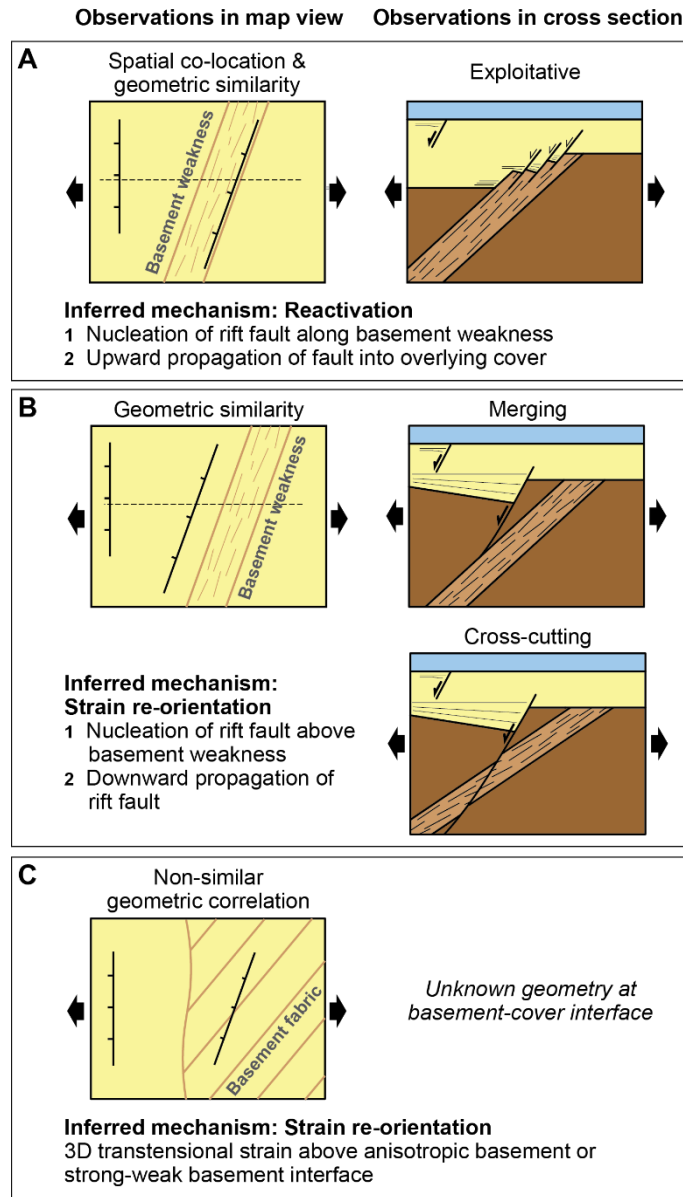
125 In this section, we summarise the spatial, geometric, and kinematic relationships between  
126 basement structures and cover faults based on observations from natural rifts.

#### 127 2.1.1. Spatial co-location and geometric similarity

128 Structural inheritance in rift basins is typically recognised through two observations in map view:  
129 *spatial co-location* and *geometric similarity* between rift-related faults and older pre-rift structures  
130 (Figure 2). **Spatial co-location** refers to the occurrence of rift-related faults above or in the vicinity  
131 of a pre-existing structure. **Geometric similarity** (sensu Holdsworth et al., 1997) is characterised  
132 by rift-related faults with traces that trend parallel to pre-rift structures (or, more rigorously, they  
133 have the same strike and dip directions in three dimensions). Both types of observations have been  
134 made at a variety of scales (Figure 3).

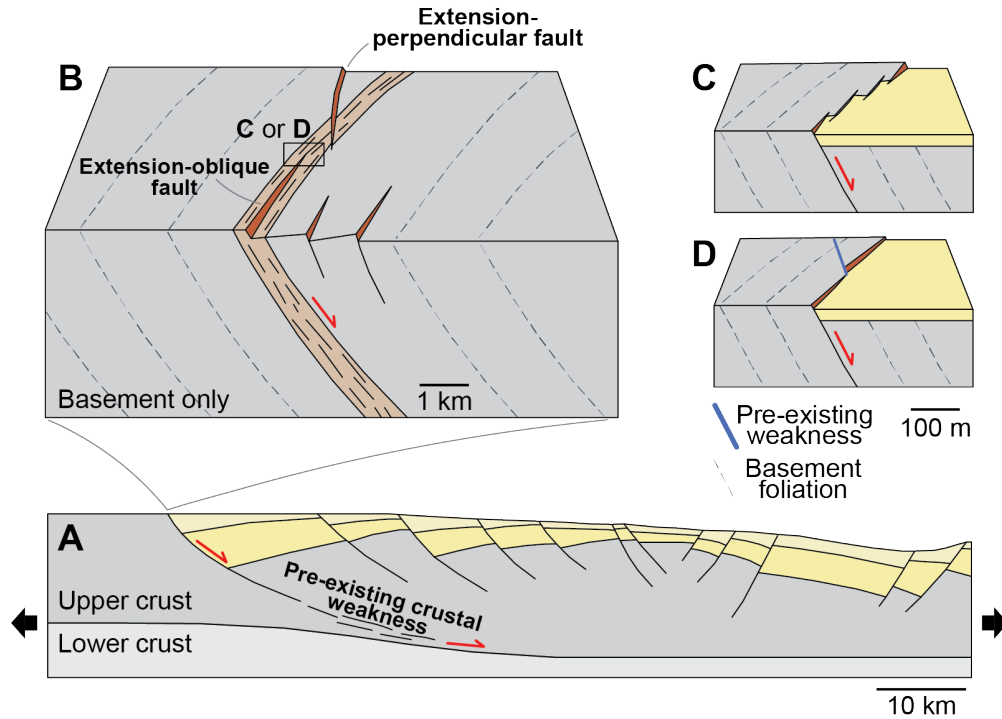
135 Plate-scale structural inheritance (a.k.a. **tectonic inheritance**; Wilson, 1966; Thomas, 2006; Audet  
136 and Bürgmann, 2011; Buitter and Torsvik, 2014; Petersen and Schiffer, 2016) is demonstrated by  
137 the co-location of pre-existing crustal or lithospheric-scale weaknesses with younger rift systems  
138 (Figure 3a). It is widely acknowledged that the exploitation of these mechanical (including  
139 thermal) weaknesses promotes rift initiation and propagation, so that younger rifts commonly  
140 follow the trends of terrane boundaries and highly deformed orogenic belts (see observations of  
141 inheritance of “Lithospheric weakness” in Table 1). We explicitly differentiate this *activation* by  
142 tectonic inheritance from *reactivation* of discrete structures. For example, most Phanerozoic rift  
143 basins in Africa are located within Proterozoic orogenic belts (Daly et al., 1989). These belts may  
144 be linked to deep-seated weaknesses in the lithospheric mantle (Tommasi and Vauchez, 2001),

145 which localise rifting in the overlying crust (Versfelt and Rosendahl, 1989). Here orogenic  
 146 structures are broadly co-located with, and geometrically similar to, historical seismic events  
 147 (Fairhead and Henderson, 1977; Sykes, 1978; Craig et al., 2011).



148

149 Figure 2 Geometric relationships between pre-existing basement structures and rift-related normal  
 150 faults in map view and cross section (exploitative, merging, and cross-cutting relationships after  
 151 Phillips et al., 2016). The inferred inheritance mechanisms behind these relationships are  
 152 reactivation (A) and strain re-orientation (B and C). Thick arrows indicate the inferred regional  
 153 extension direction during rifting.



154

155 Figure 3 The activation of a pre-existing crustal weakness influences rift-related cover faults at a  
 156 range of scales. Tectonic inheritance contributes to rift localisation (A), while basin to sub-basin  
 157 scale inheritance results in spatial co-location and geometric similarity between pre-rift structures  
 158 (e.g., basement shear zones and foliation) and rift-related normal faults (B). At the outcrop scale,  
 159 some minor faults can deviate from the main fault and crosscut basement foliation, reflecting the  
 160 complex architecture of a fault zone (C) or reactivation of other pre-existing structures, such as  
 161 dykes (D). Thick arrows indicate the inferred regional extension direction during rifting.

162 Spatial and geometric indicators of structural inheritance are also common at the basin and sub-  
 163 basin scale (Figure 3b). Several km-long basin-bounding and basin-internal faults commonly  
 164 exhibit spatial co-location and geometric similarity with pre-rift structures in the underlying  
 165 basement rocks (e.g., Laó-Dávila et al., 2015; Fazlikhani et al., 2017; Dawson et al., 2018;  
 166 Collanega et al., 2019; Wedmore et al., 2020b). For example, the strike of the Terrane Boundary  
 167 Fault in the Great South Basin (offshore South Island, New Zealand), which formed during Late  
 168 Cretaceous extension (i.e., Gondwana break-up), is parallel to the Devonian–Cretaceous Terrane  
 169 Boundary Shear Zone (Mortimer, 2004) that separates the Median Batholith and Western Province

170 terranes. Seismic reflection data show that the fault links with the crustal-scale (or potentially  
171 lithospheric-scale; e.g., Muir et al., 2000; Mortimer et al., 2002) Terrane Boundary Shear Zone at  
172 depth (Phillips and McCaffrey, 2019). Farther north in the Taranaki Basin (offshore North Island,  
173 New Zealand), the Terrane Boundary Shear Zone and an adjacent boundary between the Median  
174 Batholith and Eastern Province terranes coincide spatially with the traces of the Cenozoic Cape  
175 Egmont and Taranaki fault systems (Muir et al., 2000). Onshore, currently active N-S striking  
176 faults of the Taupō Rift (North Island, New Zealand) are parallel to terrane boundaries and bedding  
177 in the Mesozoic basement which crops out to the west and east of the rift (Villamor et al., 2017;  
178 Milicich et al., 2021).

179 In offshore southern Norway, the bounding faults of the Stavanger Basin, which formed during  
180 Permo-Triassic rifting, are parallel to and co-located with the Devonian Stavanger Shear Zone;  
181 interpreted seismic reflection data also show that the two structures are hard-linked (Phillips et al.,  
182 2016). Farther north in onshore Norway, the Lærdal-Gjende fault system is co-located and hard-  
183 linked with the Devonian Hardangerfjörd Shear Zone, which is associated with a major Moho  
184 offset (Færseth et al., 1995; Fossen and Hurich, 2005; Fossen et al., 2014). Similarly, Permo-  
185 Triassic basin-bounding rift faults in offshore Scotland exhibit geometric similarity with deep  
186 crustal reflectors in the underlying crystalline basement (Wilson et al., 2010 and references  
187 therein). From aerial imagery and field observations from northeastern Brazil, Kirkpatrick et al.  
188 (2013) found that the regional, km-scale traces of Mesozoic rift faults trend parallel to Precambrian  
189 Brasiliano shear zones and crustal-scale anomalies interpreted from magnetic and gravity data.

190 In the Upper Rhine Graben in central Europe, Bertrand et al. (2018) observed geometric similarity  
191 between magnetic foliation in magmatic basement rocks (Skrzypek et al., 2014) and km-scale horst  
192 and graben-bounding faults. There is a spatial co-location between Proterozoic NE-trending

193 basement structures of the Jemez Lineament and a rotation in fault strike in the Rio Grande Rift  
194 (United States of America) from N-NNE to ENE-E (Aldrich, 1986; Chapin et al., 2004). A growing  
195 body of work (discussed in detail in Section 3.3) provides compelling evidence that basin-scale  
196 deformation in the active East African Rift System is controlled by structural inheritance (see also  
197 a recent review on the Main Ethiopian Rift by Corti et al., 2022).

#### 198 2.1.2. Hard-link relationships between basement and cover structures

199 Phillips et al. (2016) illustrated three types of two-dimensional (2D) cross sectional relationships  
200 between a pre-existing basement shear zone and younger rift-related faults - *exploitative*, *merging*,  
201 and *cross-cutting* relationships - based on seismic reflection data from offshore southern Norway  
202 (Figure 2). These relationships were identified from basement shear zones and rift-related faults  
203 that have the same strike and dip direction. They used kinematic analyses of mapped faults to  
204 determine the history of fault activity and infer whether or not basement shear zones were  
205 reactivated as the younger faults formed.

206 Phillips et al. (2016) showed that an **exploitative** relationship is characterised by a throughgoing  
207 structure that links the basement and cover structures. Based on the physical linkage between shear  
208 zone-internal reflectors and younger rift faults, they inferred that the rift faults initiated in relatively  
209 weak mylonitic rocks (within broader shear zones) in the basement and propagated upwards into  
210 the cover. A similar observation of such an exploitative relationship was made by Collanega et al.  
211 (2019) in the Taranaki Basin (offshore North Island, New Zealand), except that it was the damage  
212 zone above a pre-existing structure that was reactivated. These two case studies suggest that  
213 reactivation (of a discrete pre-existing basement structure) is the underlying mechanism behind an  
214 exploitative basement-cover relationship (Figure 2a).

215 Merging and cross-cutting relationships (Figure 2b) differ from an exploitative relationship in that  
216 the rift-related fault nucleates above the basement structure and propagates downwards until they  
217 intersect. In a **merging relationship**, the rift-related fault nucleates within the hanging wall of the  
218 basement structure and – because of its steeper dip – merges at depth with the more gently dipping  
219 basement structure (Phillips et al., 2016). In a **cross-cutting relationship**, the rift-related fault  
220 inherits the strike and dip direction of the basement structure but offsets it at depth. For example,  
221 the Mesozoic rift-related Dombjerg Fault (East Greenland Rift System) locally strikes parallel to  
222 the more gently dipping Caledonian Kildedalen Shear Zone but offsets it farther down-dip (A.  
223 Rotevatn et al., 2018). Phillips et al. (2016) attribute merging and cross-cutting relationships to  
224 strain re-orientation by a pre-existing basement structure that has been reactivated (Figure 2b).

### 225 2.1.3. Non-similar geometric correlation

226 The influence of basement heterogeneities has also been invoked in areas where geometric  
227 similarity is not observed, but instead: (i) the strikes of coeval normal faults vary within a relatively  
228 small area (on the order of several km) (e.g., Morley et al., 2004; Reeve et al., 2015), (ii) normal  
229 fault strikes are oblique to the strikes of basement structures and not perpendicular to the inferred  
230 regional extension direction (Figure 2c) (Donath, 1962; Samsu et al., 2019), and/or (iii) fault  
231 strikes vary across areas that overlie different basement terranes (Wilson et al., 2010). In the  
232 Gippsland Basin (southeast Australia), rift-related fault orientations vary above two different  
233 basement domains. These different orientations were previously attributed to a change in rifting  
234 directions, but may instead reflect the influence of basement fabrics that are highly oblique to the  
235 inferred rifting direction (Samsu et al., 2019 and references therein). By comparing onshore fault  
236 orientations within the North Coast Transfer Zone (Scotland), Wilson et al. (2010) showed that  
237 changes in complex fault patterns in cover rocks coincide with basement terrane boundaries,

238 reflecting localised changes in three-dimensional (3D) transtensional strain in response to rifting.  
239 In the absence of evidence of basement reactivation, which is normally inferred from geometric  
240 similarity and other kinematic or chronostratigraphic indicators (Holdsworth et al., 1997), non-  
241 similar geometric correlations may indicate the subtle influence of basement rocks with fabrics  
242 that are oblique to far-field rifting directions.

#### 243 2.1.4. Basement strength variations impacting fault propagation and distribution

244 In addition to its influence on fault orientations, lateral variations in basement rock strength control  
245 the propagation and distribution of rift-related normal faults. For example, the NW trending  
246 Southern Sudan Rift terminates abruptly against the NE trending Central African fault zone, which  
247 follows the trace of the steep Late Proterozoic Fouban Shear Zone (Daly et al., 1989). Farther  
248 south, the northern tip of the western branch of the East African Rift System (trending NE at this  
249 locality) terminates against the NW trending, Mesoproterozoic Aswa Shear Zone (Katumwehe et  
250 al., 2015; Saalman et al., 2016).

251 At the basin scale, the propagation of a normal fault can be inhibited by a relatively strong  
252 basement block when the lateral boundary between the weak and strong units is at a high angle to  
253 the fault strike. In the Great South Basin (offshore South Island, New Zealand), Phillips and  
254 McCaffrey (2019) documented two styles of normal faulting near the Terrane Boundary Fault,  
255 which separates the dominantly sedimentary Western Province from the dominantly plutonic  
256 Median Batholith. Within the hanging wall of the Terrane Boundary Fault, a large-displacement  
257 normal fault within an Upper Cretaceous sedimentary unit splays into a system of low-  
258 displacement segments as it approaches a structural high in the basement comprising granitic  
259 material.



260 In other cases, where a propagating normal fault is geometrically similar to a pre-existing crustal  
261 weakness, structural inheritance can facilitate fault tip propagation and segment linkage (e.g.,  
262 Walsh et al., 2002; Jackson and Rotevatn, 2013; Rotevatn et al., 2018). This leads to the  
263 establishment of the final normal fault length at a relatively early stage (10-20%; Rotevatn et al.,  
264 2019) of its displacement history; possibly within a few earthquake cycles (Hecker et al., 2021).

#### 265 2.1.5. Scale dependence

266 The degree of influence of basement structures on cover fault orientations varies with the size of  
267 the basement structure and the scale of observation. Lithospheric and crustal-scale weaknesses  
268 localise the initiation and propagation of rifts and cause along-strike variations in rift geometry  
269 (refer to examples in Section 2.1.1 and Table 1). The activation of >1 km-long or km-wide  
270 weaknesses in lower levels of the crust can result in cover faults which are spatially co-located and  
271 geometrically similar with the reactivated weaknesses (Figure 3). Seismic reflection data from  
272 offshore areas (Phillips et al., 2016, 2021a; Collanega et al., 2019) show that this correlation results  
273 from hard linkage between relatively shallow faults and deep, pre-existing weaknesses (e.g., faults  
274 or mylonitic foliation within shear zones).

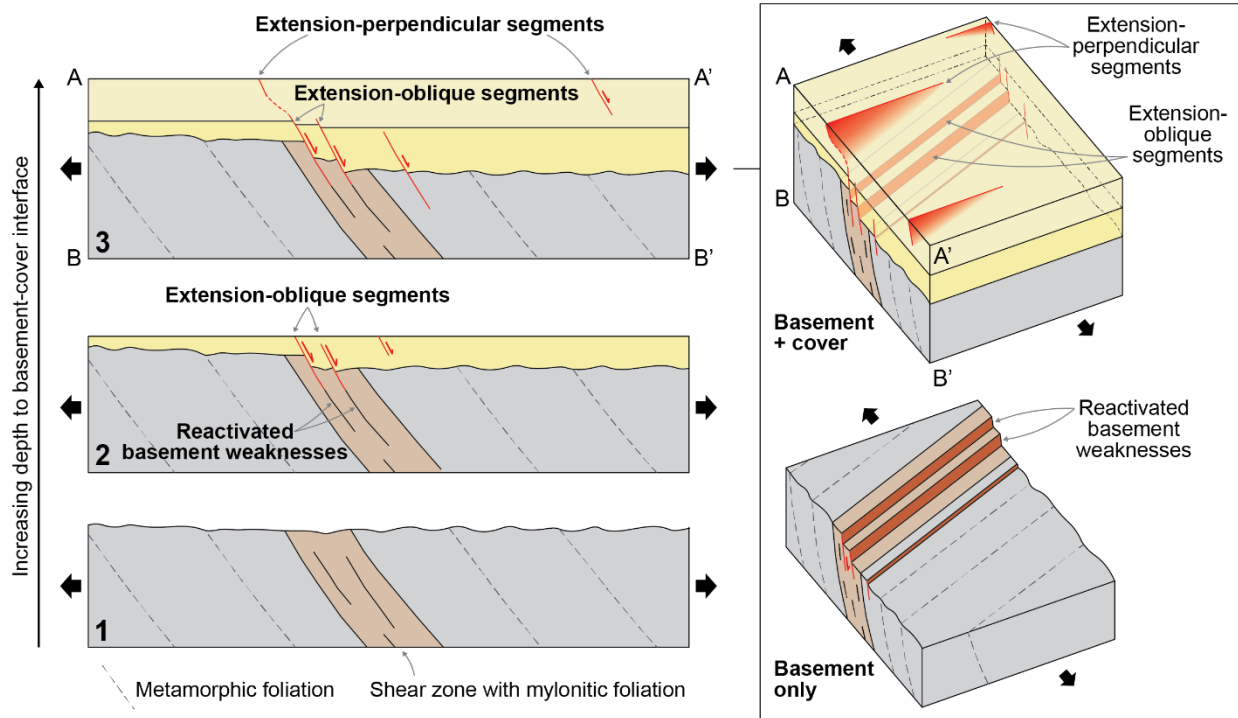
275 Rift-related faults show a more complex geometry at the sub-km scale (Figure 3c-d). Outcrop  
276 observations suggest that the influence of crustal-scale basement weaknesses is less prominent at  
277 the meters scale, which has been attributed to the increasing complexity of fault zone architecture  
278 as faults accommodate greater amounts of strain (Kirkpatrick et al., 2013). While fault initiation  
279 is controlled by grain-scale anisotropy, the coalescence of fault segments and the development of  
280 mechanically isotropic fault core rock (i.e., cataclasite and fault gouge) with increasing  
281 displacement results in complex networks of subsidiary brittle structures (Childs et al., 2009;  
282 Kirkpatrick et al., 2013; Deng et al., 2017b; Williams et al., 2022). The main fault zone therefore

283 maintains an orientation that is parallel to the basement weakness, while secondary faults deviate  
284 from the main fault trend, cross-cutting local basement foliation in some places (Figure 3c).

285 Collanega et al. (2019) documented the depth dependence of inheritance from seismic reflection  
286 data from the Taranaki Basin, where extension-oblique, intrabasement shear zones were  
287 reactivated during Plio-Pleistocene rifting. Here, rift-related faults nucleated either from  
288 intrabasement shear zones (possibly Mesozoic in age; Muir et al., 2000) or within damage zones  
289 above Late Miocene reverse faults. Collanega et al. (2019) suggested that the upward propagation  
290 of these faults into the overlying cover during rifting was controlled by the obliquity of the shear  
291 zone to the regional extension direction. Shear zones that strike perpendicular to the extension  
292 direction are hard-linked to rift-related faults that extend into the upper levels of the cover. In  
293 contrast, shear zones that strike more obliquely to the extension direction are hard-linked to rift-  
294 related faults that are restricted to the lower levels of the cover. A similar depth and orientation-  
295 dependent influence on fault orientation and linkage was observed along the reactivated, basement-  
296 rooted Parihaka Fault farther north in the Taranaki Basin (Giba et al., 2012).

297 Collanega et al. (2019) also showed that the potential for a reactivated basement weakness to  
298 localise strain and locally re-orient the far-field stress or strain can be modulated by the size of the  
299 basement weakness, i.e., the width of the weak zone. 100 m-wide zones comprising multiple  
300 discrete, mylonite-bearing faults can be reactivated and propagate upwards to shallow depths when  
301 they are nearly perpendicular to the regional extension direction. In contrast, ~1 km-wide shear  
302 zones can exert a stronger influence, reaching shallow depths, even if they are more oblique to the  
303 extension direction. The type of linkage between basement shear zones and younger faults also  
304 changes with depth. Deeper faults are hard-linked with, and geometrically similar to, the  
305 reactivated shear zone (Figure 4). Shallower faults are perpendicular to the regional extension

306 direction but form an *en échelon* arrangement parallel to basement shear zones (cf. soft linkage  
 307 between basement fault and cover fault in Phillips et al., 2021). Linkage between deep and shallow  
 308 fault segments creates an up-sequence rotation of fault strike to define a sigmoidal fault geometry  
 309 in cross section, and a twisted fault surface in 3D (Figure 4).



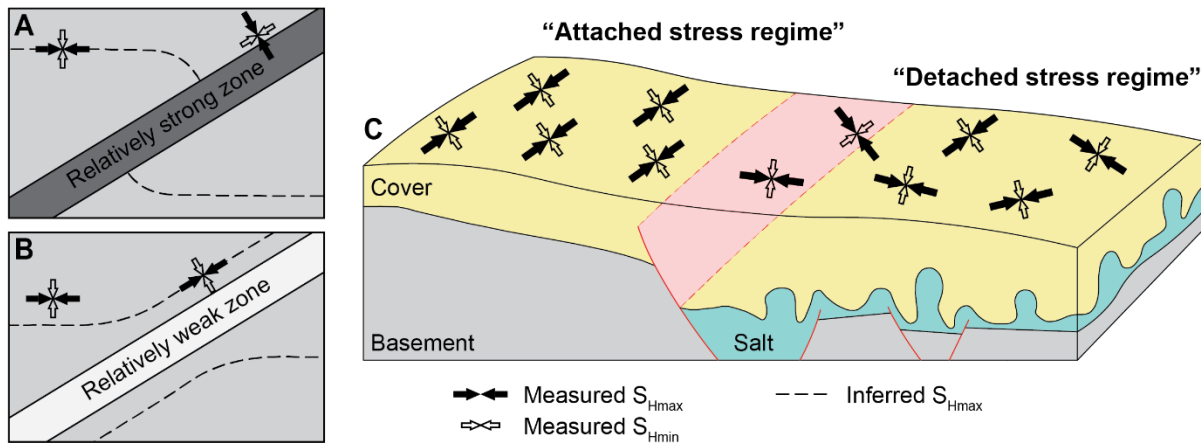
310

311 Figure 4 Conceptual illustration of depth dependence of inheritance, based on observations by  
 312 (Collanega et al., 2019). Numbers 1–3 indicate the progression of rifting and increasing thickness  
 313 of cover rocks. Faults near the basement-cover interface are geometrically similar with and rooted  
 314 in reactivated basement weaknesses (e.g., shear zone, metamorphic foliation). Shallower faults are  
 315 perpendicular to the regional extension (black arrows), suggesting that they are influenced to a  
 316 lesser degree by the basement weaknesses.

### 317 2.1.6. Stress re-orientation and coupling

318 In the brittle part of the crust, local perturbations of the regional stress field can be attributed to  
 319 lateral variations in the elastic properties of rocks (Bell, 1996 and references therein). Deviation  
 320 from the far-field or regional stress trajectories occurs because the principal stresses are deflected

321 when they cross an interface between two materials with contrasting elastic properties (e.g., Zhang  
 322 et al., 1994; Morley, 2010; Zang and Stephansson, 2010) (Figure 5). Stress perturbations around a  
 323 pre-existing weakness or discontinuity (e.g., a fault or damage zone) have been observed in  
 324 photoelastic, numerical, and rock deformation experiments. In the field, they are reflected by  
 325 curving of joints near a pre-existing fault (Cruikshank and Aydin, 1995; Muirhead and Kattenhorn,  
 326 2018; Samsu et al., 2020) or variable strain axes and kinematics of secondary, smaller-scale fault  
 327 populations around a larger fault (Riller et al., 2017). Based on in-situ horizontal stress  
 328 measurements, Yale (2003) suggested that faults are likely to perturb the regional stress field  
 329 where: (i) differential horizontal stress is small (i.e., maximum horizontal stress is not much greater  
 330 than minimum horizontal stress, usually correlating with low tectonic stress); (ii) large faults are  
 331 present, which separate the study area into distinct fault blocks; or (iii) active faulting is present.



332

333 Figure 5 Map view illustration of the re-orientation of maximum horizontal stress ( $S_{Hmax}$ ) near a  
 334 mechanically strong (A) and weak (B) zone (modified after Bell, 1996).  $S_{Hmax}$  trajectories are  
 335 perpendicular to the trend of a strong zone and parallel to the trend of a weak zone. (C) Stress  
 336 coupling between basement and cover rocks occurs in an “attached stress regime” (sensu Bell,  
 337 1996). Stress decoupling occurs when there is an intervening, mechanically weak layer (e.g.,  
 338 evaporites, overpressured shales, and low-angle faults). All figures modified after Bell (1996).

339 We can invoke basement influence on rift faults in the overlying cover by considering stress  
340 coupling between the two units. Bell (1993, 1996) proposed that stress orientations in a  
341 sedimentary unit can “exhibit the signature” of underlying rocks, provided that there is no  
342 intervening weak unit that acts as a mechanical detachment. He refers to this coupled system as an  
343 “attached stress regime” (Figure 5c) and draws on an example from the Labrador Shelf (offshore  
344 eastern Canada), where the in-situ maximum horizontal stress measured from borehole breakouts  
345 is similarly oriented to the focal mechanism P-axis of a 1971 earthquake with an epicentre located  
346 in the basement. In an attached stress regime, we can infer that any deflection or deviation of the  
347 far-field stress within the basement rocks would be transferred onto the directly overlying  
348 sedimentary unit(s) and accommodated by new brittle structures (i.e., faults and other fractures)  
349 during rifting. Such mediation of stresses from basement to cover is apparent in the Lake Rukwa  
350 area of the East African Rift System. Here, Morley (2010) suggested that the NW-SE trending  
351 Precambrian basement foliation has locally rotated the regionally dominant N-S maximum  
352 horizontal stress, resulting in similar NW-SE trends for the present-day maximum horizontal stress  
353 direction (Delvaux and Barth, 2010) and Cenozoic rift-related faults. In contrast, where a  
354 mechanically weak unit (e.g., shale-dominated unit, salt, or low-angle fault) is present between  
355 basement and cover rocks, the in-situ maximum horizontal stresses tend to show more variable  
356 orientations (“detached stress regime” in Figure 5c).

## 357 **2.2. Insights on inheritance mechanisms from analogue and numerical modelling**

358 Analogue and numerical modelling allow us to study rift and basin-forming processes over  
359 geological timescales in 2D and 3D, complementing observations from natural rifts (e.g.,  
360 Allemand and Brun, 1991; Brun, 1999; Corti, 2012; Brune et al., 2017; Molnar et al., 2020).  
361 Modelling also gives us the flexibility to examine the influence of various model parameters

362 separately (e.g., rheological layering, obliquity, geometry of inherited weakness) as well as their  
363 combined effects (Zwaan et al., 2016, 2021a, 2021b; Zwaan and Schreurs, 2017). The modelling  
364 approach is especially useful for distinguishing between the relative contributions of oblique rift  
365 kinematics and inherited structures in shaping rift basins, as each on its own can create a  
366 transtensional system, resulting in faults that are oblique to the inferred paleo-extension direction.  
367 In this section, we summarise insights from analogue and numerical models on the mechanical  
368 interaction between extension-oblique pre-rift structures and rift-related faults. Here we focus on  
369 inheritance-driven obliquity, where the model includes pre-rift weaknesses that strike obliquely to  
370 the bulk extension direction (Table 2), as opposed to boundary-driven obliquity, where bulk  
371 extension is oblique to the model boundaries (e.g., Tron and Brun, 1991; Keep and McClay, 1997;  
372 Autin et al., 2010).

373 The analogue models we discuss are simplified, multi-layer, crustal or lithospheric-scale  
374 experiments comprising a brittle upper crust, ductile lower crust, and in some examples a ductile  
375 lithospheric mantle. In this case, ‘ductile’ is defined as exhibiting spatially continuous deformation  
376 at the scale of observation, and the ductile materials simulate deformation in the viscous layers of  
377 the lithosphere, although the rheology may be different (Wang, 2021). The brittle upper crust is  
378 modelled with granular materials that exhibit frictional behaviour and follow the Mohr-Coulomb  
379 failure criterion (e.g., Hubbert, 1951; Mandl et al., 1977; Davy and Cobbold, 1991; Schellart,  
380 2000). The ductile lower crust and lithospheric mantle are modelled using materials that behave  
381 viscously under the experimental strain rates. The yield strength profile of the models resembles  
382 natural lithospheric strength profiles, which include (but are not limited to) relatively strong upper  
383 crust and lithospheric mantle layers and an intervening, weak lower crust. Pre-existing structures  
384 are implemented as two rheologically distinct blocks, discrete weak zones, or pervasive

385 anisotropies (see Table 2 for an overview). Based on these models, we discuss the impact of crustal  
386 strength variations and inherited weaknesses – with different strike orientations – on deformation  
387 localisation and partitioning. We also highlight why these models helped us to better understand  
388 how mechanical heterogeneities in the basement influence the local 3D strain field.

389 Table 2 Pre-rift crustal and mantle/lithospheric heterogeneities in nature, their influence on rift to fault-scale deformation, and their  
 390 implementation in analogue and numerical models. ‘Discrete’ and ‘pervasive’ denote the distribution of the heterogeneities at the scale  
 391 of the model.

Relevance to natural feature	Influence on deformation	Implementation in analogue model	Reference(s)	Comparable numerical models
<b><i>Crustal heterogeneity (discrete)</i></b>				
Fault or fault zone in upper crust	Fault orientation & kinematics	Zone of dilation in granular layer	Corti et al. (2007)	Deng et al. (2017b, 2018)
Shear zone in upper crust	Fault orientation & kinematics	Ductile weak zone in granular layer Cylindrical PDMS seeds at granular-ductile layer interface	Brun & Tron (1993); Osagiede et al. (2021) Zwaan et al. (2015, 2020; 2021a; 2021b); Molnar et al. (2019, 2020)	
Shear zone in lower crust	Fault orientation & kinematics; transfer zone width & orientation	Ductile weak zone in ductile layer Velocity discontinuity (rigid basal plates) Velocity discontinuity (rigid basal plate or plastic sheet separated by rubber sheet)	Corti (2008); Corti et al. (2004, 2013) Acocella et al. (1999) Withjack & Jamison (1986); McClay & White (1995)	
Pre-existing rift (thinned crust & strong lithospheric mantle)	Orientation & distribution of linkage structures between rift segments	Thin granular upper crust and ductile lower crust layers	Brune et al. (2017)	Brune et al. (2017)
Two rheologically distinct blocks	Fault spacing & propagation	Adjacent blocks with different ductile layer viscosities or thicknesses	Corti et al. (2013a); Beniest et al. (2018); Samsu et al. (2021)	Phillips et al. (2021b)
<b><i>Crustal heterogeneity (pervasive)</i></b>				
Fabric in upper crust	Fault orientation, length & kinematics	Zone of dilation in granular layer Brushed plaster at model base underneath granular layer	Bellahsen & Daniel (2005) Chattopadhyay & Chakra (2013); Ghosh et al. (2020)	
Fabric in ductile crust	Fault spacing, orientation, kinematics & propagation	Laterally alternating weak/normal zones in ductile layer	Samsu et al. (2021)	
<b><i>Mantle heterogeneity (discrete)</i></b>				
Shear zone in lithospheric mantle, terrane boundary, suture zone, orogenic belt, or thermally weakened zone in lithospheric mantle	Strain (rift) localisation; border fault orientation, length & kinematics; basin asymmetry & subsidence	Velocity discontinuity (basal plastic sheet) Weak zone in lithosphere/lithospheric mantle	Tron & Brun (1991); Brun & Tron (1993); Michon & Merle (2000); Corti et al. (2007); Zwaan et al. (2021a; 2021b) Agostini et al. (2009); Molnar et al. (2017, 2018, 2019)	Tommasi et al. (2009); Tommasi & Vauchez (2015); Petersen & Schiffer (2016)
Pre-existing rift basin	Barrier to fault propagation; fault localisation at edges	Strong zone in lithosphere/lithospheric mantle	Autin et al. (2013)	



393 2.2.1. The influence of lithospheric and crustal strength variations on strain distribution

394 The strength of the continental lithosphere and the rheology of its constituent layers exert first-  
395 order controls on the localisation of extension during rifting (Sokoutis et al., 2007). The presence  
396 of a high-strength lithospheric mantle in “cold and strong” lithosphere favours the end-member  
397 narrow rift (e.g., East African Rift System), while extension of a “hot and weak” lithosphere leads  
398 to a wide rift (e.g., Basin and Range province) (see Buck, 1991 and Brun, 1999 for a thorough  
399 discussion). Strain distribution in the cover is attributed to the coupling between the brittle and  
400 ductile layers in the model, which depends on the applied strain rate as well as the mechanical  
401 layering (i.e., thermal structure) of the lithosphere (Kusznir and Park, 1986; Cowie et al., 2005;  
402 Wijns et al., 2005; Zwaan et al., 2021b). This distribution determines where basin-bounding faults  
403 and accommodation space are created during rifting.

404 Modelling shows that rifting of heterogeneous lithosphere results in varying styles of deformation  
405 above different lithospheric or crustal blocks. Extension of two laterally juxtaposed crustal  
406 domains of different integrated strengths results in earlier strain localisation and more widely  
407 spaced and higher displacement faults in the weaker domain (Phillips et al., 2021b; Samsu et al.,  
408 2021). When the domain boundary strikes perpendicular to the extension direction, greater strain  
409 localisation above the weaker domain leads to rift margin asymmetry (Corti et al., 2013a; Beniast  
410 et al., 2018).

411 2.2.2. Activation of inheritance mechanisms depending on the orientation, depth and rheology of  
412 weaknesses: modelling insights on reactivation vs. strain re-orientation

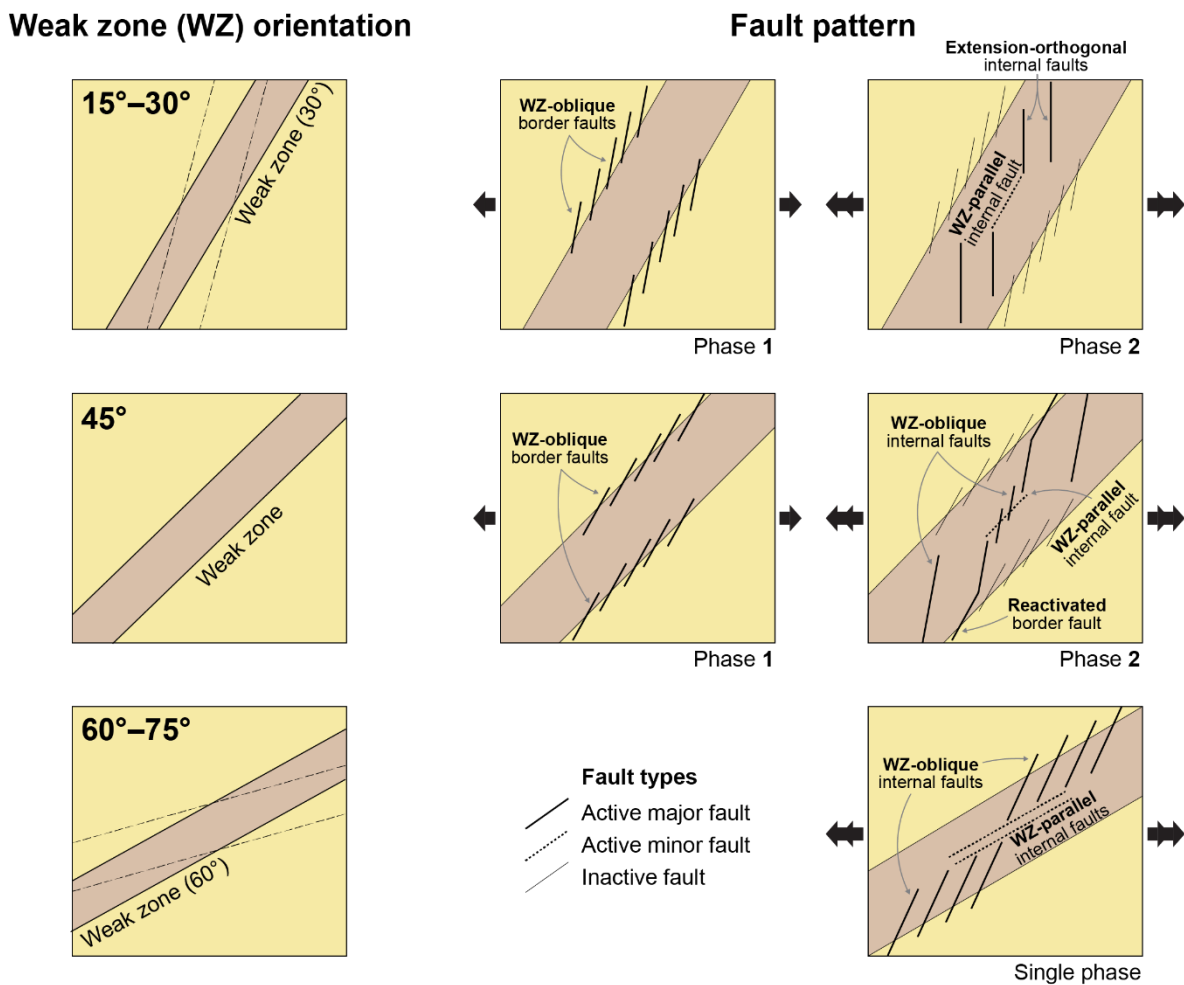
413 The (re)activation of a pre-existing weakness in a model lithosphere facilitates strain localisation  
414 and partitioning and influences the orientation of rift-related faults. Whether or not a weakness is

415 prone to (re)activation depends on several factors: (i) its obliquity with respect to the bulk  
416 extension direction, which is defined as the angle  $\alpha$  measured between the strike of the weakness  
417 and the orthogonal to the extension direction (e.g., Agostini et al., 2009); and (ii) its strength  
418 relative to surrounding rocks, which may depend on depth (i.e., the rheology of the host layer). A  
419 hierarchy of inheritance is apparent in models where discrete weaknesses of variable orientations  
420 are present in more than one layer and compete with each other to localise strain. Weaknesses in  
421 the strong upper crust and lithospheric mantle layers are preferentially (re)activated over a  
422 weakness in the relatively weak lower crust (Chenin and Beaumont, 2013; Molnar et al., 2020).  
423 When weaknesses are present in both the upper crust and lithospheric mantle, their relative  
424 contributions to strain localisation are determined by the degree of mechanical coupling between  
425 the two layers. This coupling depends on kinematic boundary conditions (e.g., rate of divergence)  
426 and the thickness and strength of the intervening, weak lower crust (Zwaan et al., 2021b).

427 Models show that discrete and pervasive weaknesses in the brittle upper crust (Brun and Tron,  
428 1993; Bellahsen and Daniel, 2005; Corti et al., 2007; Chattopadhyay and Chakra, 2013; Ghosh et  
429 al., 2020; Zwaan and Schreurs, 2020; Zwaan et al., 2021a, 2021b; see Table 2) undergo frictional  
430 reactivation (discussed from a geomechanics perspective in Section 2.3). This reactivation  
431 influences the orientations of rift-related faults (i.e., they show geometric similarity with the  
432 weaknesses) as well as their kinematics, growth, and linkage. Weaknesses that are at a high angle  
433 to the extension direction ( $\alpha < 30^\circ$ ) are reactivated in a normal sense, exhibiting mainly dip-slip  
434 kinematics and accommodating most of the extensional strain. Weaknesses that are at a lower  
435 angle to the extension direction are reactivated with a greater strike-slip component of movement;  
436 these give rise to secondary, extension-oblique faults that link the primary, extension-  
437 perpendicular faults (Bellahsen and Daniel, 2005; Osagiede et al., 2021).

438 Weaknesses in the ductile layer allow the model crust or lithosphere to locally thin more rapidly  
439 during extension, facilitating fault and graben localisation in the brittle upper crust above the  
440 weakness (Corti, 2004). By implementing a single weak zone in the ductile lithospheric mantle,  
441 some analogue models have explored the effects of weakness obliquity on fault orientations and  
442 strain localisation and partitioning, with implications for understanding inheritance at the scale of  
443 rift systems, + zone in the ductile lithospheric mantle (Corti et al., 2007; Corti, 2008, 2012;  
444 Agostini et al., 2009) or lower crust (Corti, 2004). These models show that ductile weaknesses  
445 oriented at high angles to the extension direction ( $\alpha < 45^\circ$ ) guide the map-view strike of rift  
446 segments (Corti, 2008; Agostini et al., 2009), consistent with numerical modelling of the influence  
447 of pre-existing mantle weaknesses (e.g., Tommasi et al., 2009; Tommasi and Vauchez, 2015;  
448 Petersen and Schiffer, 2016). Ductile weaknesses at low angles to the extension direction ( $\alpha > 45^\circ$ )  
449 determine where rifts are segmented and transfer zones form (e.g., Molnar et al., 2020).  
450 Deformation in the overlying brittle layer is characterised by an *en échelon* pattern of faults at the  
451 boundary between the weak and normal-strength lithosphere or crust (i.e., boundary faults) in map  
452 view. The strike of individual faults is between the main rift trend (i.e., the trend of the linear  
453 weakness) and the bulk extension direction in both low and high-obliquity rifts (Agostini et al.,  
454 2009; Corti et al., 2013b) (Figure 6). The obliquity of these faults reflects the relative contributions  
455 of extension perpendicular to the rift trend and shear parallel to the rift trend (Withjack and  
456 Jamison, 1986). Early interpretations based on fault orientations alone suggested that these faults  
457 have oblique-slip kinematics (Agostini et al., 2009), which is a response to transtension under the  
458 imposed bulk extension boundary condition. Similar studies later showed that the extension-  
459 oblique faults actually display dip-slip kinematics (Corti et al., 2013b; Philippon et al., 2015),  
460 highlighting local slip re-orientation that is associated with the underlying ductile weakness. These

461 insights from modelling support the interpretation of extension-oblique faults with dip-slip  
 462 kinematics in some natural settings, including in the Main Ethiopian Rift (Philippon et al., 2015  
 463 and references therein), the Baikal Rift (Petit et al., 1996), and the Rukwa Basin in the East African  
 464 Rift System (Delvaux et al., 2012). They also imply that strain re-orientation – an inheritance  
 465 mechanism that is different to reactivation – can occur when a pre-existing ductile weakness is  
 466 oblique to the far-field extension direction.



467

468 Figure 6 Map-view summary of analogue experiments showing differences in the evolution and  
 469 pattern of rift-related faults above a ductile weak zone (WZ) that is oblique to the imposed  
 470 extension direction (modified after Agostini et al., 2009). Thick black arrows indicate the  
 471 extension direction. Major faults are oblique to the extension direction and weak zone irrespective  
 472 of weak zone obliquity.

473 Pervasive anisotropies in the ductile layer may re-orient the far-field strain over a wider area,  
474 creating a complex pattern of extension-oblique faults in the brittle upper crust over the entire  
475 anisotropic domain. Samsu et al. (2021) presented an analogue experiment in which the  
476 orthorhombic fault pattern above a lower crustal anisotropy, oriented  $45^\circ$  to the imposed extension,  
477 is distinct from normal faults that developed above a homogeneous lower crust in the adjacent  
478 domain. They inferred that the interaction between the anisotropy and the imposed bulk extension  
479 direction resulted in localised rotation of the horizontal maximum stretching direction and non-  
480 Andersonian faulting above the anisotropic domain. The distinct fault patterns that developed  
481 above two different basement domains in this experiment are comparable with onshore fault  
482 pattern variations in the North Coast Transfer Zone (Scotland) which is underlain by basement  
483 rocks with different rheology and fabric orientations (Wilson et al., 2010). The non-coaxial vs.  
484 coaxial deformation patterns above different basement domains in these crustal-scale analogue  
485 models are also comparable with outcrop-scale observations of strain partitioning in the  
486 Carboniferous Northumberland Basin (northeast England) (De Paola et al., 2005). Here, minor  
487 faulting in the hanging wall of the reactivated Fathom Fault is partitioned into an extension-  
488 dominated regime in dolostones and wrench-dominated transtension in quartz-rich sandstones. De  
489 Paola et al. (2005) suggested that this lithological control on fault kinematics may be attributed to  
490 differences in the Poisson's ratio of different rock types.

491 Samsu et al. (2021) suggested that strain re-orientation in their experiments resulted from the  
492 strength contrast between the strong and weak domains – or in the case of an anisotropic basement,  
493 the contrast between the alternating strong and weak layers that make up the anisotropy. The strong  
494 and weak domains resist extension to different degrees, so that the difference in the rate of thinning  
495 across their boundary results in shearing at the strong-weak interface. This results in localised re-

496 orientation of the 3D strain field at: (i) the vertical interface between strong and weak crustal  
497 domains; and (ii) above basement domains which are sufficiently anisotropic (i.e., where the width  
498 of the alternating strong and weak layers is below a critical threshold).

499 Similarities between crustal-scale models and basin to outcrop-scale field observations suggest  
500 that during rifting, strain re-orientation operates at a range of length scales and requires sufficient  
501 contrast in the mechanical properties of the extended heterogeneous medium. Future experiments  
502 involving anisotropy with various orientations, different thicknesses and strength ratios of the  
503 alternating strong-weak layers, and different kinematic boundary conditions, will increase our  
504 understanding of the influence of ductile basement fabrics on upper crustal deformation at the scale  
505 of individual basins and fault systems.

### 506 **2.3. Geomechanical considerations of structural inheritance**

507 One of the mechanisms of structural inheritance that we discuss in this review – reactivation –  
508 requires some degree of movement on pre-existing planes of weakness (e.g., pre-existing faults,  
509 shear zones, pervasive fabrics, or lithological contacts). For strain re-orientation, it is less clear  
510 whether such movement is required and in which situations; nevertheless, strain re-orientation has  
511 been observed to occur in conjunction with reactivation. In this section we review the conditions  
512 under which pre-existing planes of weakness in basement rocks are expected to undergo frictional  
513 failure and potentially contribute to inheritance.

514 The tendency for frictional slip to occur on planes of weakness (as opposed to new faults nucleating  
515 in intact rock; Byerlee, 1978; Butler et al., 1997; Holdsworth et al., 1997, 2001b) in the dominantly  
516 elastic upper crust is governed by the local stress state, the orientation of the planes of weakness  
517 (Jaeger and Cook, 1979; Morris et al., 1996; Lisle and Srivastava, 2004), and the effective  
518 frictional strength of these weaknesses relative to that of surrounding intact rock. Reduced

519 effective frictional strength in pre-existing planes of weakness have been attributed to both pore  
520 fluid pressures in excess of hydrostatic fluid pressure, and lower cohesion or frictional properties  
521 due to grain-scale features such as: (a) interconnected zones of phyllosilicates or clays that provide  
522 low-friction, sliding surfaces (Byerlee, 1978; Holdsworth, 2004; Collettini et al., 2009, 2019); (b)  
523 grain boundary alignment and compositional banding (e.g., in gneisses; Shea and Kronenberg,  
524 1993; Kirkpatrick et al., 2013); and (c) high grain boundary porosity and/or low intergranular  
525 cohesion in non-foliated rocks (e.g., non-cohesive cataclasites; Sibson, 1977).

526 For a rift basin forming in an idealised Andersonian normal fault stress regime (Anderson, 1905)  
527 with a vertical maximum principal compressive stress ( $\sigma_1$ ), the fault population will be dominated  
528 by normal faults that strike perpendicular to the horizontal minimum principal compressive stress  
529 ( $\sigma_3$ ) and dip between 58-68° (Collettini and Sibson, 2001). Much of our understanding of the  
530 geomechanics of inheritance in rift settings relates to deviations from this idealised scenario, in  
531 which pre-existing structures either strike obliquely to  $\sigma_3$  and/or have a dip  $\neq$  58-68° (e.g.,  
532 Etheridge, 1986; Ranalli and Yin, 1990; Massironi et al., 2011; Williams et al., 2019). Here, we  
533 examine 2D and 3D approaches to understand how slip occurs along pre-existing planes of  
534 weakness in such cases where the dip or strike is not optimally oriented for failure and frictional  
535 sliding.

### 536 2.3.1. Influence of frictional strength and fluid pressure on basement structures

537 In the case of a pre-existing plane of weakness that strikes orthogonal to  $\sigma_3$ , the plane of weakness  
538 contains the intermediate principal compressive stress ( $\sigma_2$ ). Therefore, a 2D analysis can provide  
539 insights into the conditions required for reactivation, depending on the dip of the plane of the  
540 weakness. This analysis follows Sibson (1985), who defined an effective stress ratio for slip to  
541 occur;

542 
$$R = \frac{\sigma_1'}{\sigma_3'} = \frac{(1 + \mu_s \cot \theta)}{(1 - \mu_s \tan \theta)} \quad (1)$$

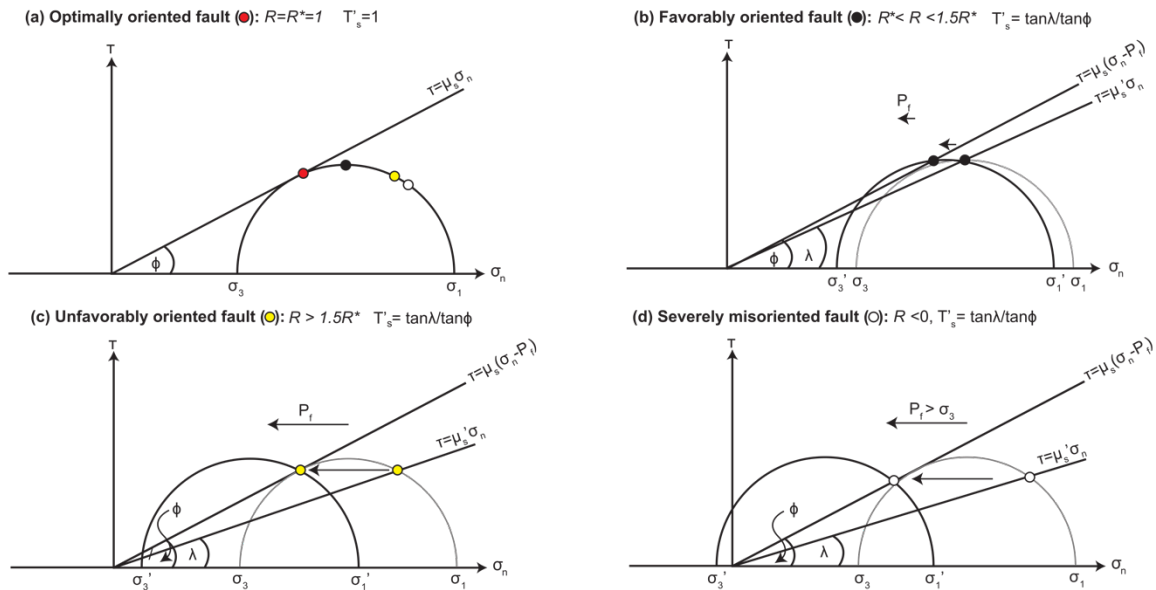
543 where  $\mu_s$  is the static coefficient of friction, which is a measure of the friction between two  
 544 cohesionless stationary surfaces that are in contact (Byerlee, 1978), and  $\sigma_1'$  and  $\sigma_3'$  are the  
 545 maximum and minimum effective principal stresses ( $\sigma_1' = \sigma_1 - P_f$  and  $\sigma_3' = \sigma_3 - P_f$ ; where  $P_f$  is the  
 546 pore fluid pressure). For pure dip-slip normal faulting in the Andersonian regime,  $\theta$  is related to  
 547 the dip of the fault or plane of weakness ( $\theta = 90 - \delta$ , where  $\delta$  is dip).

548 The approach in Equation 1 hinges on the application of a simple linear failure criterion for  
 549 cohesionless faults (Amonton's Law) containing  $\sigma_2'$  (the intermediate effective principal stress).  
 550 Alternative failure criteria can be applied that incorporate the important effect of  $\sigma_2'$  (e.g.,  
 551 Extended Griffith, Drucker-Prager; Murrell, 1963; Haimson, 2006); nevertheless, the analysis  
 552 provides a useful base case. For example, it can be used to identify three non-optimal failure  
 553 regimes (Leclère and Fabbri, 2013; Figure 7 and Figure 8a), which can be compared against the R  
 554 factor for an optimally oriented surface ( $R = R^*$ ; Figure 7a): (1) "Favourably oriented" surfaces  
 555 have dips that deviate from the optimal orientation for failure by  $\sim 15^\circ$  (e.g.,  $1-1.5R^*$ , Figure 7b).  
 556 (2) "Unfavourably oriented" surfaces have higher R values (e.g.,  $R > 1.5R^*$ ) with dips misoriented  
 557 by up to  $25-30^\circ$  from the optimal orientation (Figure 7c). (3) "Severely misoriented" surfaces are  
 558 ones that require pore fluid pressures that are greater than  $\sigma_3$  to reactivate (i.e., R is negative, Figure  
 559 7d).

560 A second outcome of Equation 1 is the significant influence of friction on the reactivation potential  
 561 of pre-existing planes of weakness in basement rocks. Laboratory measurements have yielded  
 562 friction coefficients as low as 0.2 for wet phyllosilicate and clay-rich fault gouges (Moore and  
 563 Lockner, 2004; Numelin et al., 2007), compared to 0.5-0.85 for most other Earth materials tested



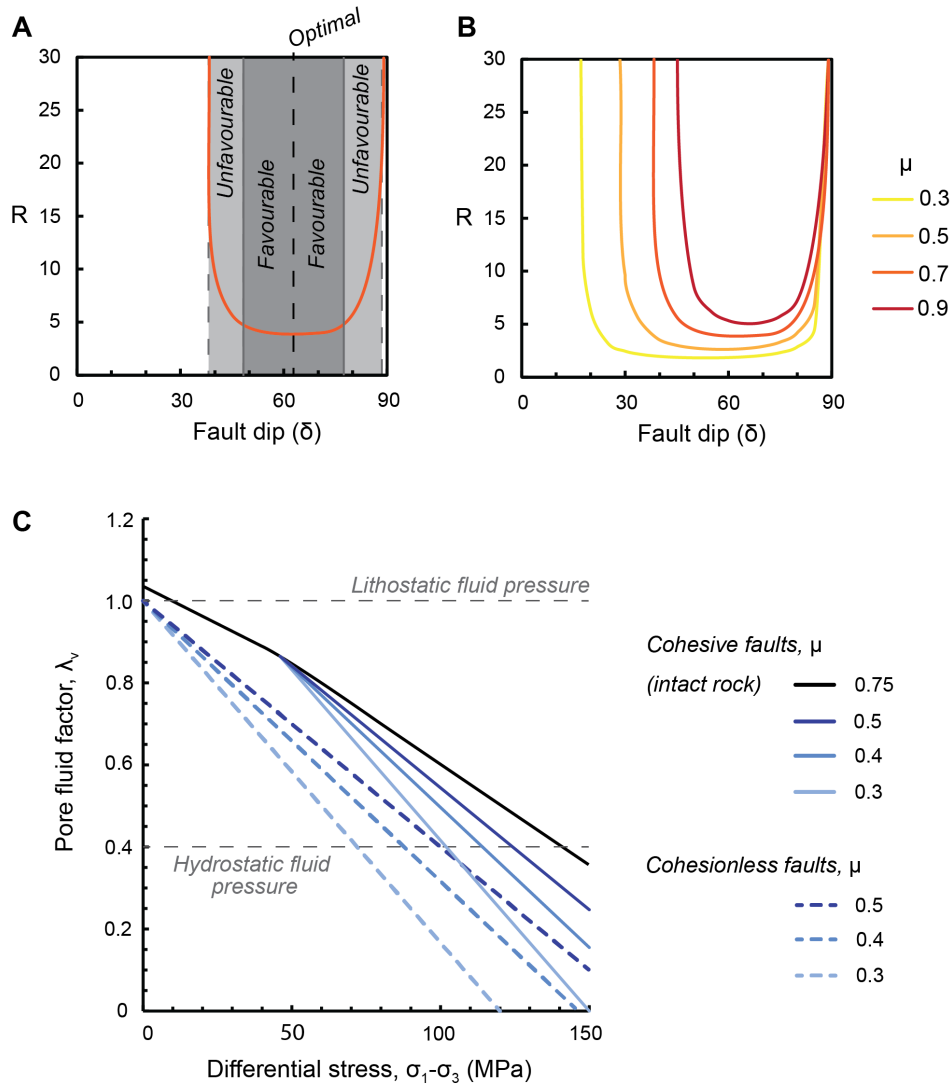
564 in wet and dry conditions (e.g., Byerlee, 1978; Jaeger et al., 2007). This means that for structures  
 565 rich in graphite, phyllosilicates, or clays (especially illite-smectite, chlorite, talc, biotite, and  
 566 pyrophyllite), such as pre-existing basement faults, the range of dips that are optimally or  
 567 favourably oriented for failure expands considerably (providing clay/phyllosilicate/graphite  
 568 content >30-60%; Numelin et al., 2007). Basement faults with coefficients of friction as low as  
 569 0.3 are therefore able to reactivate, even if their dips are as low as 25° (e.g., low angle normal  
 570 faults; e.g., Healy, 2009; Massironi et al., 2011; Demurtas et al., 2016; Singleton et al., 2018) or  
 571 nearly subvertical, without requiring elevated fluid pressure (Figure 8b).



572

573 Figure 7 Illustration in Mohr Space (i.e., plots of shear stress ( $\tau$ ) versus normal stress ( $\sigma_n$ )) for  
 574 reactivation analysis of cohesionless faults that contain  $\sigma_2$ . (a) The orientation of four faults with  
 575 different reactivation potential as quantified by their stress ratio ( $R = \sigma_1'/\sigma_3'$ ) and normalized slip  
 576 tendency ( $T'_s$ ; Lisle and Srivastava, 2004). For the case of the optimally oriented fault ( $\theta = 30^\circ$ ),  
 577  $R$  is denoted  $R^*$  and  $T'_s = 1$ . In (b)-(d),  $R$  and  $T'_s$  are schematically depicted for the reactivation of  
 578 (b) favourably oriented, (c) unfavourably oriented, and (d) severely misoriented fault. In cases (b)-  
 579 (d) a reduction in frictional strength ( $\mu_s$ ) and/or increase in pore fluid pressure ( $P_f$ ) is required for  
 580 fault reactivation. Modified after Williams et al. (2019).

581 Pore fluid factor diagrams (Figure 8c; Cox, 2010) are a useful alternate graphical method and can  
582 be used to assess the role of friction, fluid pressure, and stress on the potential for frictional sliding  
583 of basement structures. Based on this approach, Cox (2010) suggested that for the more  
584 unfavourably oriented normal faults (e.g.  $\sim 30^\circ$  dip) with a typical frictional strength ( $\mu = 0.75$ ),  
585 there is only a narrow range of differential stress in which it is possible for slip to occur on such  
586 faults, and that elevated pore fluid pressures are a pre-requisite. However, using the same approach,  
587 Figure 8c shows that when basement structures with low frictional strength are present, there is a  
588 wider range of stress conditions under which they are capable of sliding, with or without the  
589 presence of elevated fluid pressures. Figure 8b also implies that sliding on these lower friction  
590 structures can occur over a range of fault dip angles. These pre-existing weaknesses are likely to  
591 be the first structures to begin sliding at the inception of rifting and therefore have the potential to  
592 become important controls on subsequent basin geometries.



593

594 Figure 8 (A) Stress ratio required for frictional reactivation vs. fault dip for a cohesionless normal  
 595 dip-slip fault ( $\mu_s=0.7$ ), in an Andersonian regime. Shown are the dip angles for the optimal fault  
 596 orientation for (re)activation and the range of fault dips that are favourably oriented for failure.  
 597 Also shown is the range of unfavourably oriented fault dips that require elevated fluid pressures to  
 598 fail. (B) Reactivation potential for faults with low coefficients of static friction. The potential for  
 599 failure of favourably oriented faults extends over a much wider range of dips. (C) Pore fluid factor-  
 600 stress diagram (Cox, 2010), for normal dip-slip faults (10 km depth) that are optimally oriented  
 601 for each value of static friction coefficient. Basement stress states increasing from near hydrostatic  
 602 fluid pressure and low differential stress have the potential to reactivate pre-existing structures  
 603 with lower coefficients of static friction, relative to intact rock, over a wide range of stress and  
 604 fluid pressure conditions.

605 2.3.2. Extension of geomechanical analyses to 3D and implications for sedimentary basins

606 A 3D approach is required to examine the mechanics of structural inheritance when pre-existing  
607 basement structures strike obliquely to  $\sigma_3$  (i.e., the plane of weakness does not contain  $\sigma_2$ )  
608 (Williams et al., 2019). For example, ‘slip tendency analysis’ (Morris et al., 1996; Lisle and  
609 Srivastava, 2004) provides a method to estimate the potential of a cohesionless plane of weakness  
610 to activate under any stress state (Figure 7). More recently, Leclère and Fabbri (2013) introduced  
611 a 3D solution for the effective stress ratio,  $R$ , for reactivation that accounts for cohesion and does  
612 not assume an Andersonian stress regime. Relatively few studies have used this 3D approach to  
613 investigate the reactivation potential of pre-existing structures that strike obliquely to the regional  
614 extension direction. Williams et al. (2019) applied the 3D solution of Leclère and Fabbri (2013) to  
615 the southern Malawi Rift to show that weaknesses with a non-optimal strike (at an angle  $>50^\circ$  to  
616 the trend of  $\sigma_3$ ) can still reactivate, even if there is only a small difference in the strength between  
617 intact rock and moderately dipping basement weaknesses ( $\mu \sim 0.7$  and  $0.55$ - $0.65$  for intact rock  
618 and weakness respectively) or a small increase in pore fluid pressure (effective pore fluid factor  $\sim$   
619  $0.1$ - $0.3$ , i.e., sub-hydrostatic pore fluid pressures), when they have favourable dip of  $\sim 50$ - $60^\circ$  and  
620 a stress shape ratio of  $\sim 0.5$ . Hence, a wide range of strike and dip orientations and fluid pressure  
621 conditions are likely under which weak basement surfaces can be reactivated.

622 The geomechanical considerations above enable us to be more specific about the conditions in  
623 which inheritance is likely to be triggered. Basement rocks comprising metamorphosed and  
624 deformed carbonaceous shales have the potential to contain graphite-rich planes of weakness  
625 (implying low  $\mu_s = 0.2$ - $0.4$ ). Likewise, crystalline basement subjected to hydrothermal alteration  
626 or containing ultramafic rocks (ophiolites or Archean greenstone) may host phyllosilicate- and  
627 talc-rich planes of weakness.

628 It is also well established that many sedimentary basins develop elevated pore fluid pressures  
629 below a critical depth due to compaction disequilibrium and other mechanisms (Suppe, 2014;  
630 Zhang, 2019). Given that basinal fluids are known to infiltrate into the basement (Yardley et al.,  
631 2000; Gleeson et al., 2003), there are situations in which basement rocks may be saturated in  
632 hydrothermal fluids at elevated pressure. As such, elevated fluid pressures and low friction planes  
633 of weakness are common in basement rocks, meaning that structural inheritance during basin  
634 formation should be the norm rather than the exception.

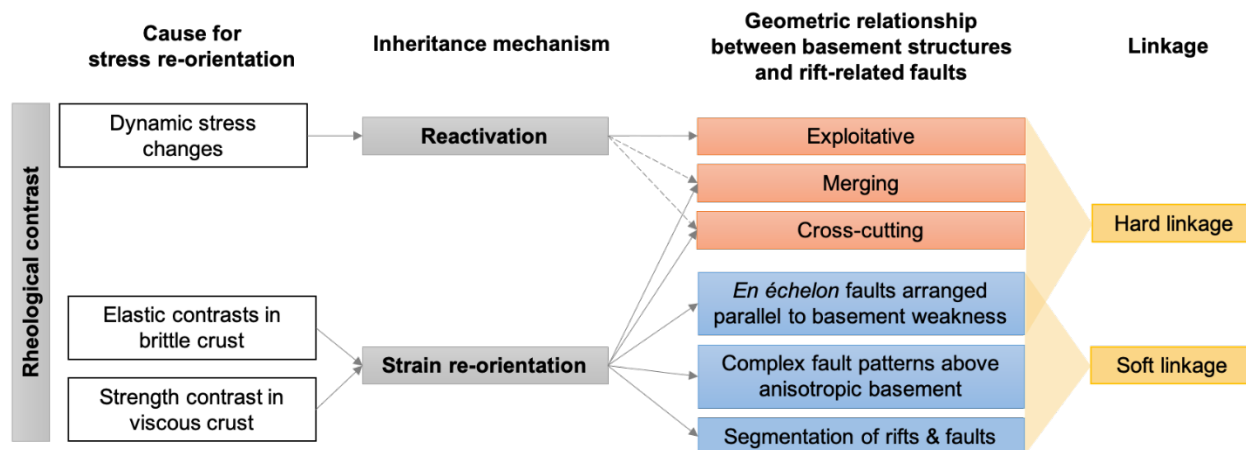
635

### 636 **3. DISCUSSION**

#### 637 **3.1. Reactivation and strain re-orientation are the two main structural inheritance** 638 **mechanisms in rift basin formation and faulting**

639 2D and 3D observations from outcrops, geophysical data, and analogue and numerical models  
640 provide insight into the interactions between pre-rift basement rocks and rift-related structures, as  
641 summarised in Section 2. This synthesis suggests that two mechanisms underpin the control of  
642 basement structures on fault orientations and geometry in the overlying basin: **reactivation** and  
643 **strain re-orientation** (Figure 9). Notably both of these mechanisms can be active during the same  
644 rift phase, either along different basement structures within the same basin, or along the same  
645 basement structure at different depths.

646



647 Figure 9 Classification of inheritance mechanisms (reactivation and strain re-orientation), their  
 648 drivers, and their expressions. Rheological contrast is a pre-requisite for both mechanisms, which  
 649 may be associated with local perturbations of the far-field stress. Such stress perturbation can be  
 650 driven by dynamic stress changes due to movement along a pre-existing weakness or by elastic  
 651 and strength contrasts in the brittle and viscously deforming crust, respectively. The two  
 652 inheritance mechanisms can be identified based on the 2D and 3D geometric relationships between  
 653 pre-rift basement structures and rift-related faults, which have been further grouped into hard and  
 654 soft linkage (referred to as hard-linked and soft-linked inheritance, respectively, in the text).

655 In the context of this discussion, reactivation implies slip along a pre-existing weak surface in the  
 656 brittle crust. During rifting, a pre-existing basement weakness can be a nucleation site from which  
 657 a new fault propagates into the overlying cover (e.g., Collanega et al., 2019) (Figure 2a). Strain re-  
 658 orientation refers to non-coaxial deformation patterns, which result from partitioning of the far-  
 659 field extensional strain at the interface between two mechanically distinct rock units (e.g., adjacent  
 660 basement domains). Bulk stretching of anisotropic basement – where the anisotropy is oblique to  
 661 the far-field stretching direction – is accommodated by different rates of extension in the strong  
 662 and weak rocks, resulting in shearing along the strong-weak boundary (e.g., Samsu et al., 2021).  
 663 Strain re-orientation can occur in conjunction with movement along a pre-existing structure (i.e.,  
 664 reactivation) (Phillips et al., 2016).

665 Both reactivation and strain re-orientation may be associated with local perturbations of the far-  
666 field stress around a pre-existing structure (i.e., local stress re-orientation) (Section 2.1.6). Stress  
667 re-orientation has been observed and modelled in three scenarios: (i) dynamic stress changes due  
668 to movement along a fault or shear zone (Barton and Zoback, 1994); (ii) deflection of stress  
669 trajectories due to elastic contrasts in the brittle crust (Figure 5a and Figure 5b) between a pre-  
670 existing structure and its host rock or between two adjacent basement domains (Bell, 1996; de  
671 Joussineau et al., 2003; Morley, 2010); and (iii) strength contrasts in the viscous crust that results  
672 in strain re-orientations (Samsu et al., 2021) which may be transmitted as stress re-orientations to  
673 an overlying mechanically coupled brittle crust. We therefore suggest that rheological contrast is  
674 a prerequisite for inheritance, which must be present for reactivation and/or strain re-orientation  
675 to occur. In sedimentary basins, a locally rotated stress field within the basement can be transferred  
676 to the overlying basin fill when the two units are mechanically coupled. If, however, an intervening  
677 weak layer separates basement and cover, then stress coupling between the basement and cover  
678 rocks is limited (Figure 5c).

679 Reactivation and strain re-orientation can occur concurrently during a single rift episode but result  
680 in different spatial and geometric relationships between the pre-existing basement structures and  
681 rift-related faults (Figure 9). Applied to the offshore southern Norway study area of Phillips et al.  
682 (2016), the distinction between these mechanisms and the extent of their influence may explain  
683 why rift-related faults exploit, merge with, or cross-cut different basement shear zones within the  
684 same basin. Strain re-orientation can also explain the occurrence of rift-related faults that form  
685 above – but do not exhibit geometric similarity with – a pre-existing basement weakness or  
686 anisotropy. The range of geometric relationships associated with strain re-orientation emphasises

687 that reactivation is not synonymous with structural inheritance, of which strain re-orientation is a  
688 common and important mechanism.

689 Whether reactivation or strain re-orientation occurs may depend on whether a pre-existing  
690 structure behaves in a frictional or viscous manner. Discrete, pre-existing weaknesses in the brittle  
691 upper crust undergo frictional reactivation when they are appropriately oriented relative to the far-  
692 field stress (Section 2.3). On the other hand, weak zones with relatively low viscosity in the viscous  
693 lower crust or lithospheric mantle influence deformation by localising and/or re-orienting strain,  
694 as demonstrated by brittle-ductile analogue models (Section 2.2.2). In natural rifts, this distinction  
695 may be used to determine whether the inherited weakness lies in the frictional or viscous crustal  
696 regimes (cf. Holdsworth et al., 2001a).

### 697 **3.2. Hard and soft-linkage classification**

698 The natural examples presented in Section 2.1 demonstrate an array of geometric relationships  
699 between pre-existing basement structures and rift-related faults (Figure 2). We suggest that these  
700 relationships can be classified into hard- and soft-linked inheritance, to denote whether a rift-  
701 related fault is physically connected to a pre-existing basement structure (Figure 9): **Hard-linked**  
702 **inheritance** is characterised by a physical link between a pre-existing basement structure and a  
703 younger, rift-related fault in the sedimentary cover. **Soft-linked inheritance** is defined as the  
704 apparent influence of a pre-existing basement structure on a rift-related fault, where a physical link  
705 between the two is not observed. We note that this classification does not describe the genetic  
706 relationship between the pre-existing and rift-related structures or the inheritance mechanism  
707 (Figure 9).

#### 708 3.2.1. Hard-linked inheritance



709 A shallow fault and a deeper, pre-existing structure are classified as hard-linked if they have  
710 identical strike and dip direction and an exploitative, merging, or cross-cutting relationship (sensu  
711 Phillips et al., 2016; Section 2.1.2) (Figure 9). This classification is based on observations made  
712 in cross section, where there is a physical connection between the rift-related fault and the pre-  
713 existing structure. An exploitative relationship (Figure 2a) relies on reactivation of a pre-existing  
714 weakness, associated with previous fault or shear zone-forming processes. A merging relationship  
715 (Figure 2b) involves strain re-orientation and may involve some degree of reactivation; in the  
716 example documented by Phillips et al. (2016), the basement structure did not exhibit significant  
717 rift-related displacement at the scale of observation. Similarly, hard-linked inheritance may apply  
718 to examples of the cross-cutting relationship where the rift-related fault inherits the strike and dip  
719 direction of the basement structure (Rotevatn et al., 2018).

720 The relative contributions of strain re-orientation and reactivation mechanisms to the merging and  
721 cross-cutting relationships described above are exemplified by rift-related normal faults that inherit  
722 the strike of a nearby, pre-existing basement shear zone with a gentler dip than the rift-related  
723 normal faults (e.g., Fazlikhani et al., 2017; Rotevatn et al., 2018; Osagiede et al., 2020). Geometric  
724 similarity between the rift-related faults and a pre-existing shear zone may be initiated by strain  
725 re-orientation, for example caused by a grain-scale mechanical anisotropy that formed in the same  
726 deformation event as the shear zone (Kirkpatrick et al., 2013). Such a pervasive fabric records  
727 distributed strain, and movement along the weak layers within the fabric enables strain re-  
728 orientation. Evidence from in-situ stress measurements and earthquake focal mechanisms suggest  
729 that such strain re-orientation is associated with local re-orientation of the far-field maximum (and  
730 minimum) horizontal stress trajectories by the mechanically weak zones (Bell, 1996; Morley,  
731 2010).

732 Geometric similarity, in association with hard-linked inheritance, may be limited to deeper cover  
733 units, which are closer to the pre-existing basement structure. This depth-dependent relationship  
734 is demonstrated by rift-related faults that are segmented and oblique to a pre-existing basement  
735 structure in the upper part of the cover but appear to merge into a continuous structure striking  
736 parallel to the basement structure at depth (Deng et al., 2017b; Collanega et al., 2019). The shallow  
737 faults exhibit an *en échelon* arrangement that strikes parallel to the basement structure and  
738 perpendicular to the far-field extension direction (Figure 4). In-situ stress measurements show that  
739 changes in fault strike with increasing vertical distance from a pre-existing basement weakness  
740 can be attributed to local stress re-orientation by the basement structure, which is mechanically  
741 weak compared to the surrounding rock (Tingay et al., 2010b). Near the surface, the far-field  
742 stresses have a greater influence than at depth (Yale, 2003), contributing to shallow rift-related  
743 faults that strike perpendicular to the minimum horizontal far-field stress.

#### 744 3.2.2. Soft-linked inheritance

745 The *Soft-linked inheritance* classification applies when rift-related faults are spatially co-located  
746 with a mapped basement structure, but the fault strikes are oblique to both the basement structure  
747 and inferred regional extension direction (e.g., Samsu et al., 2019) and/or we cannot observe a  
748 hard linkage between the basement structure and rift-related fault in cross section (e.g., Phillips et  
749 al., 2021). Analogue experiments suggest that such ‘misoriented’ faults form when the pre-existing  
750 basement structures behave in a viscous as opposed to frictional manner during rifting, regardless  
751 of whether they are discrete or pervasive. Models with a discrete weakness in the ductile lower  
752 crust, which strikes  $\leq 45^\circ$  relative to the extension direction, demonstrate the formation of  
753 extension-oblique faults in the overlying crust (Agostini et al., 2009; Corti et al., 2013b) (Figure  
754 6). Dip-slip kinematics and slip re-orientation along the extension-oblique faults (Philippon et al.,

755 2015) reflect strain re-orientation near the boundary between the weaker and stronger lower crust  
756 domains and in the overlying upper crust. Strain re-orientation can also occur across a wider area  
757 when the analogue ductile basement is mechanically anisotropic, with pervasive, closely spaced  
758 weaknesses that are oblique to the far-field extension direction (Samsu et al., 2021). The anisotropy  
759 gives rise to transtensional strain, even under boundary conditions that simulate orthogonal rifting,  
760 resulting in sets of non-Andersonian faults with traces that are oblique to the anisotropy in map  
761 view.

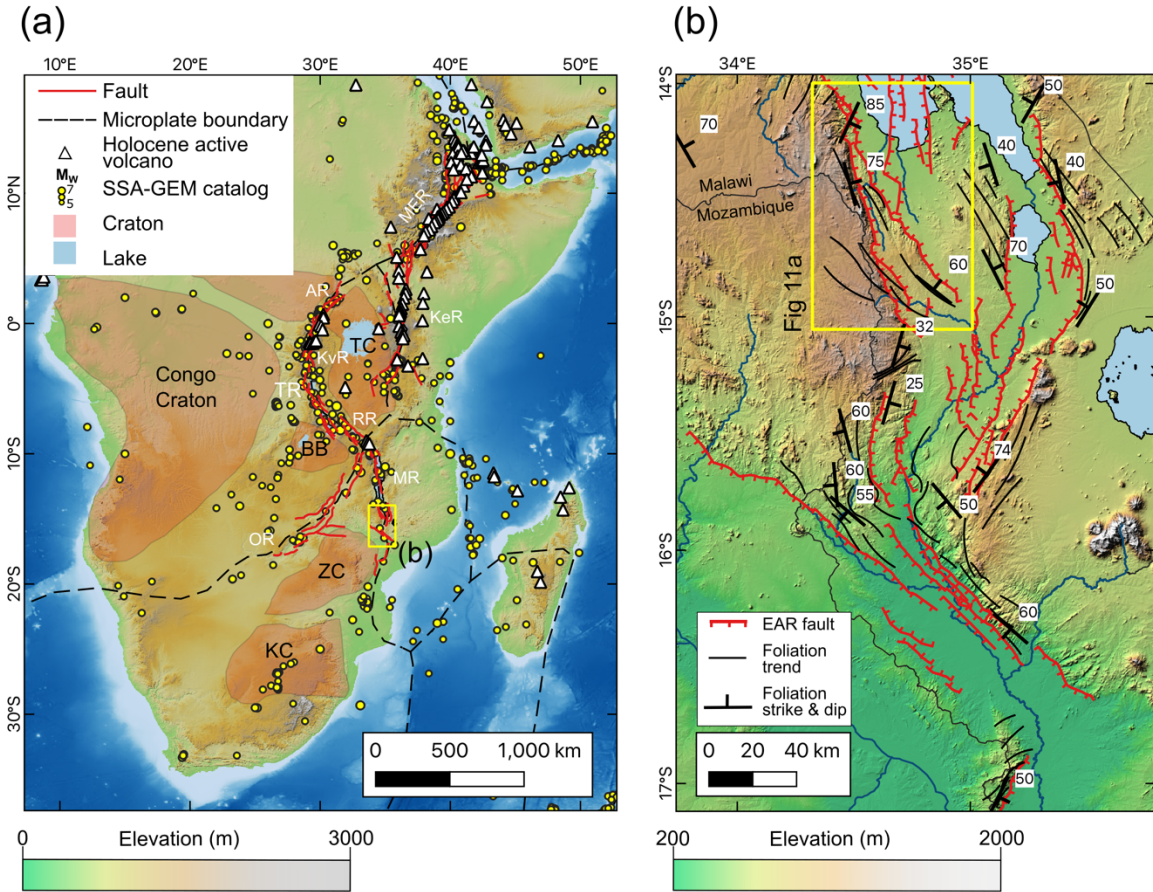
762 The presence of a relatively weak, ductile layer (e.g., clay, salt) can decouple the basement from  
763 cover units, as observed in seismic reflection data and through in-situ stress measurements (Bell,  
764 1996). Where an intervening weak layer is present between two cover units, this decoupling effect  
765 can result in a combination of soft-linked and hard-linked inheritance. In this case, the basement  
766 weakness is geometrically similar to rift-related faults below the mechanically weak layer but  
767 geometrically dissimilar to an *en échelon* fault array above the weak layer (e.g., Jackson and  
768 Rotevatn, 2013; Roche et al., 2020; Phillips et al., 2021a).

769 The spatial co-location of inferred, deep-seated basement structures with transfer zones (a.k.a.  
770 accommodation zones) that separate distinct rift segments and basins (e.g., Rowland and Sibson,  
771 2004; Fossen et al., 2016) can also be described as soft-linked inheritance. The absence of cover  
772 faults parallel to the inferred basement structures imply that the basement structures were not  
773 directly reactivated and are not hard-linked to any of the rift-related faults. Therefore, we can infer  
774 that the basement structure, which strikes at a high angle to the main rift trend, is not favourably  
775 oriented for reactivation but locally re-orientes the far-field extension direction. While it is widely  
776 acknowledged that such pre-existing structures contribute to continental-scale rift segmentation,

777 there is scope for further exploring the relationship between soft-linked inheritance and the  
778 formation of sub-basin-scale relay structures (Fossen and Rotevatn, 2016).

### 779 **3.3. Applying the structural inheritance framework to the East African Rift System**

780 The East African Rift System (EARS) is the pre-eminent example of an active continental rift,  
781 exhibiting all stages of continental rift evolution from nascent seafloor spreading in Afar to  
782 incipient faulting in the Okavango Rift of Botswana (Figure 10a; McConnell, 1972; Chorowicz,  
783 2005; Ebinger, 2005; Macgregor, 2015; Daly et al., 2020). Hard- and soft-linked structural  
784 inheritance has influenced the evolution of the EARS at many spatial scales (and also magma  
785 emplacement mechanisms and volcanic activity; see Corti et al., 2022 for examples from the Main  
786 Ethiopian Rift). A famous example of plate-scale inheritance is present south of the Main  
787 Ethiopian Rift, where the Eastern and Western Branches of the EARS wrap around the relatively  
788 rigid Archean Tanzanian craton and spatially co-locate with orogenic belts that formed during the  
789 progressive Proterozoic amalgamation of the African Continent (Figure 10a; Daly et al., 1989;  
790 Versfelt and Rosendahl, 1989; Nyblade and Brazier, 2002; Corti et al., 2007). New geodetic and  
791 geologic evidence indicates that this is just one of several cases of plate-scale structural inheritance  
792 where the EARS bifurcates to co-locate with pre-existing weak zones around Archean cratons; in  
793 this context, the EARS represents inheritance of relatively weak, deformed Proterozoic lithosphere  
794 bounding more rigid blocks (Figure 10a; Daly et al., 2020; Stamps et al., 2021; Wedmore et al.,  
795 2021).



796

797 Figure 10 Plate and basin scale structural inheritance in the East African Rift System (EARS). (a)  
 798 Distribution of active faults (Hodge et al., 2018; Daly et al., 2020; Styron and Pagani, 2020),  
 799 microplate boundaries (Wedmore et al., 2021), Holocene volcanoes (Global Volcanism Project,  
 800 2013), earthquake events ( $M_w \geq 5$ , 1875-2015) from the Sub-Saharan Africa Global Earthquake  
 801 Model (SSA-GEM) catalogue (Poggi et al., 2017), and Archean-Paleoproterozoic cratons in the  
 802 EARS (Van Hinsbergen et al., 2011). MER; Main Ethiopian Rift; KeR, Kenya Rift; AR, Albertine  
 803 Rift; KvR, Kivu Rift; TR; Tanganyika Rift RR, Rukwa Rift; MR, Malawi Rift; OR, Okavango  
 804 Rift; TC; Tanzanian Craton; BB, Bangweulu Block; ZC, Zimbabwe Craton; KC, Kaapvaal Craton.  
 805 (b) Surface traces of faults and foliation in southern Malawi (Williams et al., 2019, 2021b;  
 806 Kolawole et al., 2021a). Foliation trends and strike and dip measurements from (Williams et al.,  
 807 2019 and references therein). (a) Underlain by GTOPO30 Digital Elevation Model (DEM) and (b)  
 808 by Shuttle Radar Topography Mission DEM (Sandwell et al., 2011).

809 At the ~10-100 km scale, the EARS can be divided along strike into distinct half-graben or graben  
 810 basins. It is debated whether the along-strike extent of these basins is guided by the intrinsic  
 811 strength of the lithosphere or pre-existing rift-perpendicular structures (Ebinger et al., 1987;

812 Ebinger, 1989; Upcott et al., 1996; Katumwehe et al., 2015; Laó-Dávila et al., 2015; Heilman et  
813 al., 2019; Scholz et al., 2020; Corti et al., 2022); nevertheless, in either case the patterns of faulting  
814 within these basins can be linked to structural inheritance. The most commonly described  
815 examples are fault traces that are subparallel to surface foliations (i.e., ‘geometric similarity’)  
816 imparted by Proterozoic orogenic events in East Africa, as observed, for example, in the Malawi  
817 (Ring, 1994; Laó-Dávila et al., 2015; Dawson et al., 2018; Hodge et al., 2018; Kolawole et al.,  
818 2018; Williams et al., 2019; Scholz et al., 2020; Shillington et al., 2020; Wedmore et al., 2020b),  
819 Albertine (Katumwehe et al., 2015), Kivu (Smets et al., 2016), Kenya (Smith and Mosley, 1993;  
820 Robertson et al., 2016; Muirhead and Kattenhorn, 2018), the Main Ethiopian (Corti et al., 2022),  
821 Okavango (Kinabo et al., 2007), and Rukwa Rifts (Morley, 2010; Delvaux et al., 2012; Heilman  
822 et al., 2019; Kolawole et al., 2021b). East Africa also experienced a Mesozoic (or ‘Karoo’) phase  
823 of rifting related to Gondwana fragmentation. The segmentation and orientation of Karoo  
824 structures was also affected by Proterozoic structures and fabrics (Ring, 1994; Delvaux, 2001;  
825 Paton, 2006; Bingen et al., 2009). In turn, Karoo structures have been reactivated during East  
826 African rifting (Castaing, 1991; Macgregor, 2015; Daly et al., 2020; Wedmore et al., 2020b) or  
827 have influenced rift segmentation (Accardo et al., 2018), depending on their orientation relative to  
828 the regional stresses.

829 The 3D geometric relationship between faults and fabrics in the EARS at depth is uncertain;  
830 however, it is likely that where fabrics are moderately dipping (e.g., southern Malawi Rift;  
831 Wedmore et al., 2020) relationships are exploitative (sensu Phillips et al., 2016), whilst merging  
832 or cross-cutting relationships are present in regions where the fabrics are subvertical (e.g., northern  
833 Malawi Rift; Dawson et al., 2018; Kolawole et al., 2018). Geometric similarity is not ubiquitous  
834 within the EARS. For example, faults in the Tanganyika Rift and central Malawi Rift are not

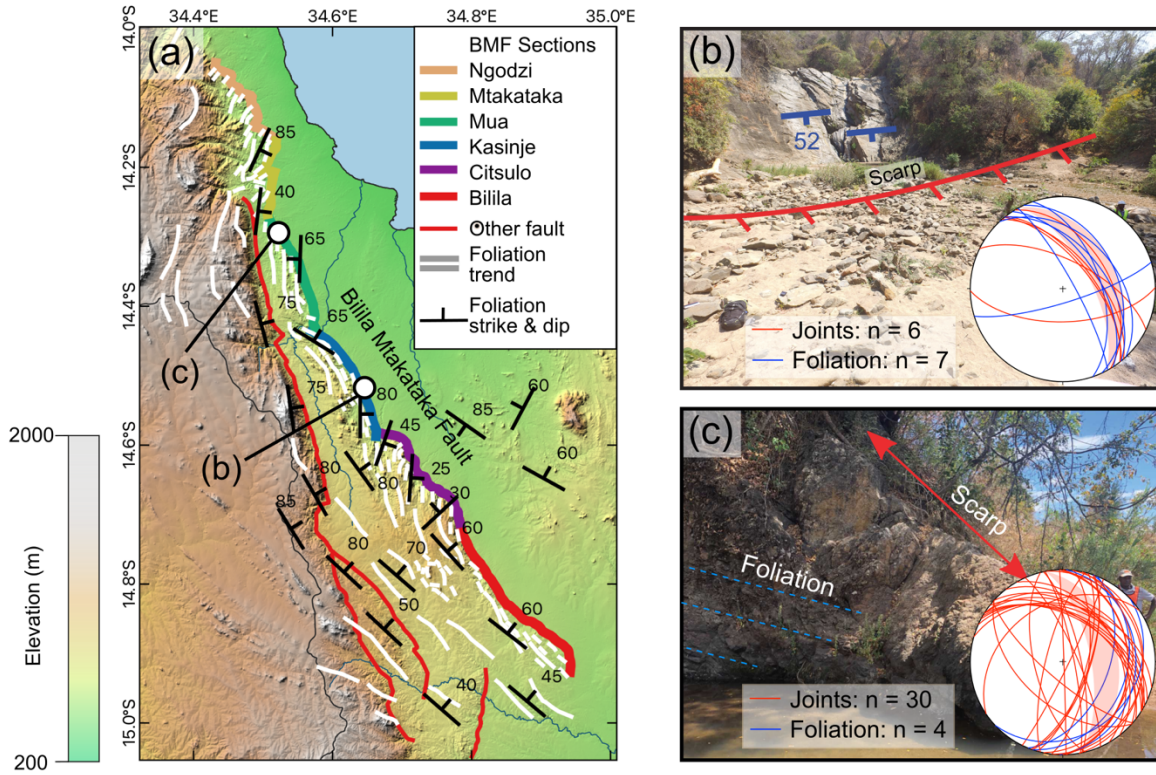
835 parallel to surrounding crustal fabrics (Muirhead et al., 2019; Scholz et al., 2020), and the degree  
836 to which metamorphic fabrics influence fault orientations can change as rift extension progresses  
837 (Muirhead and Kattenhorn, 2018; Nutz et al., 2022). Furthermore, local variations in fabric  
838 orientation may disrupt geometric similarity at the scale of an individual fault, resulting in faults  
839 that locally cross-cut fabrics, along-strike fault segmentation, and/or faults that are Z-shaped in  
840 plan-view due to scarps that are continuous across perpendicular bends (Figure 11; Hodge et al.,  
841 2018; Corti et al., 2022).

842 When invoking a mechanism for the geometric similarity in the EARS it is not always clear if: (1)  
843 fabrics are non-optimally oriented to the regional extensional direction, but reactivate because they  
844 are frictionally weak and/or incohesive (i.e., hard-linked exploitative reactivation, Figure 2a;  
845 (Dawson et al., 2018; Wedmore et al., 2020), (2) fabrics are optimally oriented to the regional  
846 extension direction and so geometric similarity is a coincidence (Baker et al., 1972; Smith and  
847 Mosley, 1993), or (3) non-optimally oriented fabrics are actively rotating the local (i.e., at the scale  
848 of the fault; Twiss and Unruh, 1998) extension direction, so that foliation-parallel faults exhibit  
849 dip-slip displacement despite striking oblique to the regional extension direction (Tingay et al.,  
850 2010b; Corti et al., 2013b, 2022; Muirhead and Kattenhorn, 2018; Williams et al., 2019). Analogue  
851 models imply that the latter is an example of soft-linked structural inheritance as these local  
852 extension directions reflect deep-seated (not surface or shallow) weaknesses in the crust (Corti et  
853 al., 2013b; Philippon et al., 2015). Therefore, mechanisms (1) and (3) could apply at different  
854 depths to the same fault (Hodge et al., 2018; Wedmore et al., 2020b).

855 Structural inheritance in the EARS is not limited to geometric similarity. For example, as rift  
856 extension proceeds in the EARS, it is typically observed that strain migrates from large basin-  
857 bounding faults to a network of smaller intrabasin faults in the rift valley (Ebinger, 2005). Early

858 localisation of rift-related strain onto a border fault may be facilitated by the exploitation of a  
859 discrete pre-existing weakness (e.g., a terrane boundary or basement viscous shear zone; Wheeler  
860 and Karson, 1989; Katumwehe et al., 2015; Scholz et al., 2020; Wedmore et al., 2020b; Kolawole  
861 et al., 2021b). Alternatively, pervasive lateral heterogeneities in the crust (e.g., a wide  
862 anastomosing shear zone) can promote distributed deformation involving migration of extensional  
863 strain from the basin boundary to intrabasin faults (Kolawole et al., 2018, 2021b; Wedmore et al.,  
864 2020a). Normal fault lengthening by exploitation of pre-existing fabrics (Section 2.1.4; Walsh et  
865 al., 2002) may account for why faults in the EARS achieved their full length at an early stage of  
866 their displacement accumulation (Vétel et al., 2005; Accardo et al., 2018; Corti et al., 2019; Ojo et  
867 al., 2022) and exhibit narrow fault damage zones and large single-earthquake displacement-to-  
868 length ratios (Figure 11) (Hodge et al., 2020; Williams et al., 2022). An important observation at  
869 the < 100 km scale is therefore that although the EARS is a classic example of plate-scale structural  
870 inheritance and co-location with relatively weak lithosphere (e.g., Versfelt and Rosendahl, 1989),  
871 this inheritance is not synonymous with reactivation. Instead, reactivation is limited to where  
872 discrete, relatively weak structures are available in an orientation that is favourable for reactivation  
873 as the dominant (frictional or viscous) deformation mechanism (Wheeler and Karson, 1989;  
874 Kolawole et al., 2018; Heilman et al., 2019). However, at depths or locations where such structures  
875 are not available, the orientations and dimensions of new structures are locally variable and likely  
876 related to basement anisotropy (Hodge et al., 2018; Williams et al., 2019; Wedmore et al., 2020b).





877

878 Figure 11 Fault-scale structural inheritance in the EARS using the example of the Bilila-Mtakataka  
 879 Fault (BMF) in the southern Malawi Rift (Jackson and Blenkinsop, 1997; Hodge et al., 2018). (a)  
 880 Map of the BMF and surrounding surface foliation orientations (Hodge et al., 2018 and references  
 881 therein). The relative orientation of the fault, surrounding foliation, and along strike minima in  
 882 fault scarp height have been used to divide it into the shown segments (Hodge et al., 2018). Extent  
 883 of figure shown in Figure 10b. Field examples of where the BMF is (b) parallel and (c) oblique to  
 884 the surrounding foliation (Williams et al., 2022). Equal area stereonets indicate relative  
 885 orientations of foliation and joints in the fault's surrounding damage zone, shaded area indicates  
 886 local trend of BMF scarp and a range of plausible fault dips (40-65°; Hodge et al., 2018; Stevens  
 887 et al., 2021; Williams et al., 2022).

888 Seismic hazard investigation is a practical application for the study of structural inheritance in the  
 889 EARS. For example, the influence of structural inheritance on the distribution of extensional strain  
 890 between border and intrarift faults will dictate whether regions of high seismic hazard are in the  
 891 basin interior or along the margin(s) (Dawson et al., 2018; Wedmore et al., 2020a; Williams et al.,  
 892 2021b). Pre-existing crustal fabrics may also modulate the along-strike segmentation of faults, and  
 893 this can affect whether faults rupture in relatively frequent, moderate-magnitude segmented fault

894 ruptures, or more uncommon whole-fault ruptures (Biasi and Wesnousky, 2016; Hodge et al.,  
895 2018; Wedmore et al., 2020b).

#### 896 **3.4. Implications of structural inheritance for natural resources**

897 The activation of pre-existing weaknesses during rifting has wide ranging implications from a geo-  
898 energy and minerals exploration perspective, some of which are highlighted in this section. The  
899 extraction of geothermal energy and the formation of hydrothermal mineral systems rely on  
900 hydrothermal fluid circulation, which is affected by the spatiotemporal pattern of deformation. For  
901 example, heat and mass transfer from deep sources to shallower depths are facilitated by  
902 convection through networks of open fractures (e.g., Rowland and Simmons, 2012). These  
903 fractures are especially important in rocks with low primary porosity and permeability, such as  
904 crystalline basement. At the plate scale, tectonic inheritance controls the location and lithology of  
905 sedimentary basins as well as the preservation of fluid pathways between deep heat and metal  
906 sources and shallow reservoirs (e.g., Hoggard et al., 2020). At the basin scale, rifting can bring  
907 about favourable stress conditions for reactivating pre-existing faults as permeable fractures.

908 The Upper Rhine Graben is an example of a deep geothermal system where the most permeable  
909 reservoir is located at the top of the granitic basement (e.g., Vidal and Genter, 2018; Glaas et al.,  
910 2021). NNW-SSE to N-E striking Variscan faults and fabrics in the basement may have been  
911 reactivated in a normal sense during the basin's multiphase history of Cenozoic regional shortening  
912 and extension (e.g., Schumacher, 2002), contributing to thick (i.e., wide-aperture) fractures with  
913 enhanced permeability (Glaas et al., 2021). Bertrand et al. (2018) show that in the Upper Rhine  
914 Graben, pre-existing faults, fabrics, and lithologies can impact fracture patterns at certain scales  
915 but not in others, demonstrating that the impact of inheritance on flow modelling is scale  
916 dependent. Structural mapping, with an aim to understand the multi-scale controls of inheritance

917 on fractures, has been applied to other geothermal systems, including in France (Dezayes et al.,  
918 2010), Mexico (Norini et al., 2019), and the UK (Yeomans et al., 2020).

919 In the Taupō Volcanic Zone (New Zealand), structural inheritance appears to control shallow  
920 geothermal systems and the formation of hydrothermal gold and silver deposits at <2,000 m depths  
921 (i.e., epithermal ore deposits). Upwelling of hot water plumes is enhanced at the intersections of  
922 mapped or inferred structures, including faults, basement-controlled transfer zones, and caldera  
923 boundaries (Rowland and Sibson, 2004; Rowland and Simmons, 2012; Villamor et al., 2017;  
924 Milicich et al., 2021). Rowland and Sibson (2004) associated the segmentation of the NNE-SSW  
925 trending rift system, via so-called accommodation zones, with WNW-ESE trending basement  
926 structures interpreted from geophysics. The same geometric relationship has also been inferred for  
927 the similarly NNE-SSW trending Coromandel Volcanic Zone farther north (Bahiru et al., 2019).  
928 Rowland and Simmons (2012) suggested that such basement structures may be physically linked  
929 with potentially permeable shear zones in the lower crust, enabling fluid transport across the  
930 brittle-ductile transition zone (Cox et al., 2001), though at present there is no evidence of hard  
931 linkage between the basement structures and shallower rift-related structures.

932 Inheritance of lithospheric boundaries and crustal-scale weaknesses during rifting contributes to  
933 the formation of world-class sediment-hosted base metal deposits (i.e., copper, lead, zinc, and  
934 nickel) near craton edges (e.g., Mount Isa, Australia; Gibson et al., 2016; Hoggard et al., 2020).

935 Here, the long-lived nature of the craton edge is attributed to focusing of deformation over multiple  
936 extensional and contractional events. Rifting of thick cratonic lithosphere facilitates the formation  
937 of deep, widely spaced faults that remain active (through reactivation) for up to 100 Myr,  
938 extending the time window for mineralisation (Allen and Armitage, 2012) and the distribution of  
939 basin fill lithologies that are conducive to mineralisation (Hoggard et al., 2020 and references

940 therein). In addition, reactivation of crustal structures maintains focused fluid flow between the  
941 deep and shallow levels of basins (Gibson et al., 2016).

942 Our understanding of tectonic inheritance and fault/fabric reactivation have been integrated into  
943 studies on rift evolution and basin formation in the context of paleotectonic reconstructions (e.g.,  
944 Gouiza and Paton, 2019; Heron et al., 2019) and hydrocarbon exploration (e.g., Morley, 1995;  
945 Lyon et al., 2007; Whipp et al., 2014). Studies on the East African Rift System have also  
946 demonstrated the role of inherited structures in modulating seismic hazard (refer to Section 3.3).  
947 The examples we discuss here suggest that there is scope for applying our knowledge of  
948 lithospheric and crustal-scale controls of inheritance to geothermal and mineral systems, which  
949 can contribute to successful exploration and development of geothermal energy, base metals, and  
950 critical metals. Basement structure characterisation and quantification of the reactivation potential  
951 of pre-existing fractures (including faults) under in-situ stresses must also be implemented in  
952 geothermal drilling projects (Deichmann and Giardini, 2009; Diehl et al., 2017), in addition to  
953 exploring the feasibility of geological storage of CO<sub>2</sub> (e.g., Andrés et al., 2016) and nuclear waste  
954 (e.g., Barton and Zoback, 1994) to support the current energy transition.

#### 955 **4. CONCLUSION**

956 Compositional heterogeneities and mechanical discontinuities in pre-deformed crust can locally  
957 alter the local stress or strain field. This structural inheritance, which has been observed from the  
958 plate scale down to the outcrop scale, is probably the norm rather than exception, and it influences  
959 the location and geometries of entire rift systems, basins, and faults during rifting. Lithospheric  
960 and crustal-scale zones of weakness facilitate localised thinning, contributing to the formation and  
961 propagation of rifts along inherited higher strain belts. At the same scale, accommodation zones  
962 are spatially co-located with inferred deep-seated structures that strike at high angles to the main

963 rift. The boundaries and evolution of rift basins are controlled by boundary faults that, if  
964 inconsistent with the far-field strain, may indicate exploitation of a reactivated basement weakness  
965 and/or reflect a locally re-oriented strain field above a deep, potentially viscously deforming  
966 structure. Individual faults at the sub-basin scale may also exploit weak surfaces in the basement  
967 or a pre-existing rift fabric. Some faults may appear to be unaffected by inheritance and reflect the  
968 far-field regional extension, suggesting that the vertical and lateral extents of stress and strain re-  
969 orientation are limited by the depth, size, orientation, and strength (relative to the surrounding  
970 rocks) of the pre-existing structure.

971 Based on our review of previous field and modelling work, we have distilled observations of  
972 structural inheritance into two key mechanisms: reactivation and strain re-orientation. One or both  
973 of these mechanisms are activated when extension affects two mechanically distinct basement  
974 terranes or occurs in the presence of an anomalously weak (or strong) structure within relatively  
975 homogeneous-strength basement rock. Reactivation is generally associated with geometric  
976 similarity and hard linkage between the pre-existing structure and the younger, rift-related fault.  
977 These observations are consistent with many of the expressions of inheritance found around the  
978 world, most notably in the Atlantic and the East African Rift System (Table 1). However, strain  
979 re-orientation is invoked when it comes to certain observations of soft linkage, particularly where  
980 a rift-related fault is oblique to a pre-existing structure (e.g., Tingay et al., 2010b; Giba et al., 2012;  
981 Collanega et al., 2019; Phillips et al., 2021a). While strain re-orientation is not as readily  
982 recognisable as reactivation, further understanding of the conditions under which strain re-  
983 orientation applies can help us explain the presence of complex fault patterns in rift basins, better  
984 constrain the far-field paleostrain in ancient rifts, and more confidently map basement structures  
985 under cover.

986 **ACKNOWLEDGEMENTS**

987 A. Samsu is supported by the Australian Research Council Linkage grant LP190100146 which  
988 was awarded to A.R. Cruden.

989

990 **REFERENCES**

- 991 Accardo, N.J., Shillington, D.J., Gaherty, J.B., Scholz, C.A., Nyblade, A.A., Chindandali, P.R.N.,  
992 Kamihanda, G., McCartney, T., Wood, D., Wambura Ferdinand, R., 2018. Constraints on Rift  
993 Basin Structure and Border Fault Growth in the Northern Malawi Rift From 3-D Seismic  
994 Refraction Imaging. *Journal of Geophysical Research: Solid Earth* 123, 3-10,10,25.  
995 <https://doi.org/10.1029/2018JB016504>
- 996 Agostini, A., Corti, G., Zeoli, A., Mulugeta, G., 2009. Evolution, pattern, and partitioning of  
997 deformation during oblique continental rifting: Inferences from lithospheric-scale centrifuge  
998 models. *Geochemistry, Geophysics, Geosystems* 10. <https://doi.org/10.1029/2009GC002676>
- 999 Aldrich, M.J., 1986. Tectonics of the Jemez lineament in the Jemez Mountains and Rio Grande  
1000 Rift ( USA). *Journal of Geophysical Research* 91, 1753–1762.  
1001 <https://doi.org/10.1029/JB091iB02p01753>
- 1002 Allemand, P., Brun, J.-P., 1991. Width of continental rifts and rheological layering of the  
1003 lithosphere. *Tectonophysics* 188, 63–69. [https://doi.org/10.1016/0040-1951\(91\)90314-I](https://doi.org/10.1016/0040-1951(91)90314-I)
- 1004 Allen, P.A., Armitage, J.J., 2012. Cratonic basins. In: Busby, C., Azor, A. (Eds.), *Tectonics of*  
1005 *Sedimentary Basins: Recent Advances*. Blackwell Publishing, 602–620.
- 1006 Anderson, E.M., 1905. The dynamics of faulting. *Transactions of the Edinburgh Geological*

- 1007 Society 8, 387–402. <https://doi.org/https://doi.org/10.1144/transed.17.3.217>
- 1008 Andrés, J., Alcalde, J., Ayarza, P., Saura, E., Marzán, I., Martí, D., Catalán, J.R.M., Carbonell, R.,  
1009 Pérez-Estaún, A., Garića-Lobón, J.L., Rubio, F.M., 2016. Basement structure of the  
1010 Hontomín CO<sub>2</sub>storage site (Spain) determined by integration of microgravity and 3-D  
1011 seismic data. *Solid Earth* 7, 827–841. <https://doi.org/10.5194/se-7-827-2016>
- 1012 Ashby, D.E., 2013. Influences on Continental Margin Development: A Case Study from the Santos  
1013 Basin, south-eastern Brazil. Durham University. PhD Thesis.
- 1014 Audet, P., Bürgmann, R., 2011. Dominant role of tectonic inheritance in supercontinent cycles.  
1015 *Nature Geoscience* 4, 184–187. <https://doi.org/10.1038/ngeo1080>
- 1016 Autin, J., Bellahsen, N., Husson, L., Beslier, M.O., Leroy, S., D’Acremont, E., 2010. Analog  
1017 models of oblique rifting in a cold lithosphere. *Tectonics* 29, 1–23.  
1018 <https://doi.org/10.1029/2010TC002671>
- 1019 Bahiru, E.A., Rowland, J. V., Eccles, J.D., Kellett, R.L., 2019. Regional crustal-scale structural  
1020 control on epithermal deposits within the Hauraki Goldfield, Coromandel Volcanic Zone,  
1021 New Zealand: insight from integrated geological and aeromagnetic structural patterns. *New  
1022 Zealand Journal of Geology and Geophysics* 62, 461–482.  
1023 <https://doi.org/10.1080/00288306.2019.1574268>
- 1024 Baker, B.H., Mohr, P.A., Williams, L.A.J., 1972. Geology of the Eastern Rift System of Africa.  
1025 *GSA Special Papers*. 1–68. <https://doi.org/10.1130/SPE136-p1>
- 1026 Barton, C.A., Zoback, M.D., 1994. Stress perturbations associated with active faults penetrated by  
1027 boreholes: Possible evidence for near-complete stress drop and a new technique for stress

- 1028 magnitude measurement. *Journal of Geophysical Research: Solid Earth* 99, 9373–9390.  
1029 <https://doi.org/10.1029/93JB03359>
- 1030 Bell, J.S., 1996. Petro geoscience 2. In situ stresses in sedimentary rocks (part 2): Applications of  
1031 stress measurements., *Geoscience Canada*.
- 1032 Bell, J.S., 1993. Attached and detached in-situ stress regimes in sedimentary basins. 5th  
1033 Conference & Technical Exhibition. European Association of Petroleum Geoscientists &  
1034 Engineers, Stavanger, Norway, 7-11 June 1993, F046. [https://doi.org/10.3997/2214-](https://doi.org/10.3997/2214-4609.201411772)  
1035 [4609.201411772](https://doi.org/10.3997/2214-4609.201411772)
- 1036 Bellahsen, N., Daniel, J.M., 2005. Fault reactivation control on normal fault growth: An  
1037 experimental study. *Journal of Structural Geology* 27, 769–780.  
1038 <https://doi.org/10.1016/j.jsg.2004.12.003>
- 1039 Beniést, A., Willingshofer, E., Sokoutis, D., Sassi, W., 2018. Extending continental lithosphere  
1040 with lateral strength variations: Effects on deformation localization and margin geometries.  
1041 *Frontiers in Earth Science* 6, 1–11. <https://doi.org/10.3389/feart.2018.00148>
- 1042 Bertrand, L., Jusseaume, J., Géraud, Y., Diraison, M., Damy, P.-C., Navelot, V., Haffen, S., 2018.  
1043 Structural heritage, reactivation and distribution of fault and fracture network in a rifting  
1044 context: Case study of the western shoulder of the Upper Rhine Graben. *Journal of Structural*  
1045 *Geology* 108, 243–255. <https://doi.org/10.1016/j.jsg.2017.09.006>
- 1046 Biasi, G.P., Wesnousky, S.G., 2016. Steps and Gaps in Ground Ruptures: Empirical Bounds on  
1047 Rupture Propagation. *Bulletin of the Seismological Society of America* 106, 1110–1124.  
1048 <https://doi.org/10.1785/0120150175>



- 1049 Bingen, B., Jacobs, J., Viola, G., Henderson, I.H.C., Skår, Boyd, R., Thomas, R.J., Solli, A., Key,  
1050 R.M., Daudi, E.X.F., 2009. Geochronology of the Precambrian crust in the Mozambique belt  
1051 in NE Mozambique, and implications for Gondwana assembly. *Precambrian Research* 170,  
1052 231–255. <https://doi.org/10.1016/j.precamres.2009.01.005>
- 1053 Bird, P.C., Cartwright, J.A., Davies, T.L., 2014. Basement reactivation in the development of rift  
1054 basins: an example of reactivated Caledonide structures in the West Orkney Basin. *Journal of*  
1055 *the Geological Society* 172, 77–85. <https://doi.org/10.1144/jgs2013-098>
- 1056 Bladon, A.J., Clarke, S.M., Burley, S.D., 2015. Complex rift geometries resulting from inheritance  
1057 of pre-existing structures: Insights and regional implications from the Barmer Basin rift.  
1058 *Journal of Structural Geology* 71, 136–154. <https://doi.org/10.1016/j.jsg.2014.09.017>
- 1059 Brun, J.P., 1999. Narrow rifts versus wide rifts: Inferences for the mechanics of rifting from  
1060 laboratory experiments. *Philosophical Transactions of the Royal Society A: Mathematical,*  
1061 *Physical and Engineering Sciences* 357, 695–712. <https://doi.org/10.1098/rsta.1999.0349>
- 1062 Brun, J.P., Tron, V., 1993. Development of the North Viking Graben: inferences from laboratory  
1063 modelling. *Sedimentary Geology* 86, 31–51. [https://doi.org/10.1016/0037-0738\(93\)90132-O](https://doi.org/10.1016/0037-0738(93)90132-O)
- 1064 Brune, S., Corti, G., Ranalli, G., 2017. Controls of inherited lithospheric heterogeneity on rift  
1065 linkage: Numerical and analogue models of interaction between the Kenyan and Ethiopian  
1066 rifts across the Turkana depression. *Tectonics* 1–20. <https://doi.org/10.1002/2017TC004739>
- 1067 Buck, W.R., 1991. Modes of Continental Lithospheric Extension. *Journal of Geophysical Research*  
1068 96, 20161–20178. <https://doi.org/10.1029/91JB01485>
- 1069 Buitter, S.J.H., Torsvik, T.H., 2014. A review of Wilson Cycle plate margins: A role for mantle

1070 plumes in continental break-up along sutures? *Gondwana Research* 26, 627–653.  
1071 <https://doi.org/10.1016/j.gr.2014.02.007>

1072 Butler, R.W.H., Holdsworth, R.E., Lloyd, G.E., 1997. The role of basement reactivation in  
1073 continental deformation. *Journal of the Geological Society* 154, 69–71.  
1074 <https://doi.org/10.1144/gsjgs.154.1.0069>

1075 Byerlee, J., 1978. Friction of rocks. *Pure and Applied Geophysics* 116, 615–626.  
1076 <https://doi.org/10.1007/BF00876528>

1077 Castaing, C., 1991. Post-Pan-African tectonic evolution of South Malawi in relation to the Karroo  
1078 and recent East African rift systems. *Tectonophysics* 191, 55–73.  
1079 [https://doi.org/10.1016/0040-1951\(91\)90232-H](https://doi.org/10.1016/0040-1951(91)90232-H)

1080 Chapin, C.E., Wilks, M., McIntosh, W.C., 2004. Space--time patterns of Late Cretaceous to  
1081 present magmatism in New Mexico—comparison with Andean volcanism and potential for  
1082 future volcanism. *New Mexico Bureau of Geology and Mineral Resources Bulletin* 160, 13–  
1083 40.

1084 Chattopadhyay, A., Chakra, M., 2013. Influence of pre-existing pervasive fabrics on fault patterns  
1085 during orthogonal and oblique rifting: An experimental approach. *Marine and Petroleum*  
1086 *Geology* 39, 74–91. <https://doi.org/10.1016/j.marpetgeo.2012.09.009>

1087 Chenin, P., Beaumont, C., 2013. Influence of offset weak zones on the development of rift basins:  
1088 Activation and abandonment during continental extension and breakup. *Journal of*  
1089 *Geophysical Research: Solid Earth* 118, 1698–1720. <https://doi.org/10.1002/jgrb.50138>

1090 Childs, C., Manzocchi, T., Walsh, J.J., Bonson, C.G., Nicol, A., Schöpfer, M.P.J., 2009. A

- 1091 geometric model of fault zone and fault rock thickness variations. *Journal of Structural*  
1092 *Geology* 31, 117–127. <https://doi.org/10.1016/j.jsg.2008.08.009>
- 1093 Chorowicz, J., 2005. The East African rift system. *Journal of African Earth Sciences* 43, 379–410.  
1094 <https://doi.org/10.1016/j.jafrearsci.2005.07.019>
- 1095 Collanega, L., Siuda, K., A.-L. Jackson, C., Bell, R.E., Coleman, A.J., Lenhart, A., Magee, C.,  
1096 Breda, A., 2019. Normal fault growth influenced by basement fabrics: The importance of  
1097 preferential nucleation from pre-existing structures. *Basin Research* 31, 659–687.  
1098 <https://doi.org/10.1111/bre.12327>
- 1099 Collettini, C., Sibson, R.H., 2001. Normal faults, normal friction? *Geology* 29, 927–930.  
1100 [https://doi.org/10.1130/0091-7613\(2001\)029<0927:NFNF>2.0.CO;2](https://doi.org/10.1130/0091-7613(2001)029<0927:NFNF>2.0.CO;2)
- 1101 Collettini, C., Tesei, T., Scuderi, M.M., Carpenter, B.M., Viti, C., 2019. Beyond Byerlee friction,  
1102 weak faults and implications for slip behavior. *Earth and Planetary Science Letters* 519, 245–  
1103 263. <https://doi.org/10.1016/j.epsl.2019.05.011>
- 1104 Collettini, C., Viti, C., Smith, S.A.F., Holdsworth, R.E., 2009. Development of interconnected talc  
1105 networks and weakening of continental low-angle normal faults. *Geology* 37, 567–570.  
1106 <https://doi.org/10.1130/G25645A.1>
- 1107 Corti, G., 2012. Evolution and characteristics of continental rifting: Analog modeling-inspired  
1108 view and comparison with examples from the East African Rift System. *Tectonophysics* 522–  
1109 523, 1–33. <https://doi.org/10.1016/j.tecto.2011.06.010>
- 1110 Corti, G., 2008. Control of rift obliquity on the evolution and segmentation of the main Ethiopian  
1111 rift. *Nature Geoscience* 1, 258–262. <https://doi.org/10.1038/ngeo160>

- 1112 Corti, G., 2004. Centrifuge modelling of the influence of crustal fabrics on the development of  
1113 transfer zones: Insights into the mechanics of continental rifting architecture. *Tectonophysics*  
1114 384, 191–208. <https://doi.org/10.1016/j.tecto.2004.03.014>
- 1115 Corti, G., Cioni, R., Franceschini, Z., Sani, F., Scaillet, S., Molin, P., Isola, I., Mazzarini, F., Brune,  
1116 S., Keir, D., Erbello, A., Muluneh, A., Illsley-Kemp, F., Glerum, A., 2019. Aborted  
1117 propagation of the Ethiopian rift caused by linkage with the Kenyan rift. *Nature*  
1118 *Communications* 10, 1309. <https://doi.org/10.1038/s41467-019-09335-2>
- 1119 Corti, G., Iandelli, I., Cerca, M., 2013a. Experimental modeling of rifting at craton margins.  
1120 *Geosphere* 9, 138–154. <https://doi.org/10.1130/GES00863.1>
- 1121 Corti, G., Maestrelli, D., Sani, F., 2022. Large-to Local-Scale Control of Pre-Existing Structures  
1122 on Continental Rifting : Examples From the Main Ethiopian Rift , East Africa. 10, 1–18.  
1123 <https://doi.org/10.3389/feart.2022.808503>
- 1124 Corti, G., Philippon, M., Sani, F., Keir, D., Kidane, T., 2013b. Re-orientation of the extension  
1125 direction and pure extensional faulting at oblique rift margins: Comparison between the Main  
1126 Ethiopian Rift and laboratory experiments. *Terra Nova* 25, 396–404.  
1127 <https://doi.org/10.1111/ter.12049>
- 1128 Corti, G., van Wijk, J., Cloetingh, S., Morley, C.K., 2007. Tectonic inheritance and continental rift  
1129 architecture: Numerical and analogue models of the East African Rift system. *Tectonics* 26,  
1130 1–13. <https://doi.org/10.1029/2006TC002086>
- 1131 Cowie, P.A., Underhill, J.R., Behn, M.D., Lin, J., Gill, C.E., 2005. Spatio-temporal evolution of  
1132 strain accumulation derived from multi-scale observations of Late Jurassic rifting in the  
1133 northern North Sea: A critical test of models for lithospheric extension. *Earth and Planetary*

- 1134 Science Letters 234, 401–419. <https://doi.org/10.1016/j.epsl.2005.01.039>
- 1135 Cox, S.F., 2010. The application of failure mode diagrams for exploring the roles of fluid pressure  
1136 and stress states in controlling styles of fracture-controlled permeability enhancement in  
1137 faults and shear zones. *Geofluids* 10, 217–233. [https://doi.org/10.1111/j.1468-](https://doi.org/10.1111/j.1468-8123.2010.00281.x)  
1138 [8123.2010.00281.x](https://doi.org/10.1111/j.1468-8123.2010.00281.x)
- 1139 Cox, S.F., Knackstedt, M.A., Braun, J., 2001. Principles of Structural Control on Permeability and  
1140 Fluid Flow in Hydrothermal Systems. In: Richards, J.P., Tosdal, R.M. (Eds.), *Structural*  
1141 *Controls on Ore Genesis*. Society of Economic Geologists, 1–24.
- 1142 Craig, T.J., Jackson, J.A., Priestley, K., McKenzie, D., 2011. Earthquake distribution patterns in  
1143 Africa: Their relationship to variations in lithospheric and geological structure, and their  
1144 rheological implications. *Geophysical Journal International* 185, 403–434.  
1145 <https://doi.org/10.1111/j.1365-246X.2011.04950.x>
- 1146 Cruikshank, K.M., Aydin, A., 1995. Unweaving the joints in Entrada Sandstone, Arches National  
1147 Park, Utah, U.S.A. *Journal of Structural Geology* 17, 409–421. [https://doi.org/10.1016/0191-](https://doi.org/10.1016/0191-8141(94)00061-4)  
1148 [8141\(94\)00061-4](https://doi.org/10.1016/0191-8141(94)00061-4)
- 1149 Daly, M.C., Chorowicz, J., Fairhead, J.D., 1989. Rift basin evolution in Africa: the influence of  
1150 reactivated steep basement shear zones. Geological Society, London, Special Publications 44,  
1151 309–334. <https://doi.org/10.1144/GSL.SP.1989.044.01.17>
- 1152 Daly, M.C., Green, P., Watts, A.B., Davies, O., Chibesakunda, F., Walker, R., 2020. Tectonics  
1153 and Landscape of the Central African Plateau and their Implications for a Propagating  
1154 Southwestern Rift in Africa. *Geochemistry, Geophysics, Geosystems* 21.  
1155 <https://doi.org/10.1029/2019GC008746>

- 1156 Davy, P., Cobbold, P.R., 1991. Experiments on shortening of a 4-layer model of the continental  
1157 lithosphere. *Tectonophysics* 188, 1–25. [https://doi.org/10.1016/0040-1951\(91\)90311-F](https://doi.org/10.1016/0040-1951(91)90311-F)
- 1158 Dawson, S.M., Laó-Dávila, D.A., Atekwana, E.A., Abdelsalam, M.G., 2018. The influence of the  
1159 Precambrian Mughese Shear Zone structures on strain accommodation in the northern  
1160 Malawi Rift. *Tectonophysics* 722, 53–68. <https://doi.org/10.1016/j.tecto.2017.10.010>
- 1161 de Joussineau, G., Petit, J.P., Gauthier, B.D.M., 2003. Photoelastic and numerical investigation of  
1162 stress distributions around fault models under biaxial compressive loading conditions.  
1163 *Tectonophysics* 363, 19–43. [https://doi.org/10.1016/S0040-1951\(02\)00648-0](https://doi.org/10.1016/S0040-1951(02)00648-0)
- 1164 De Paola, N., Holdsworth, R.E., McCaffrey, K.J.W., 2005. The influence of lithology and pre-  
1165 existing structures on reservoir-scale faulting patterns in transtensional rift zones. *Journal of*  
1166 *the Geological Society* 162, 471–480. <https://doi.org/10.1144/0016-764904-043>
- 1167 Deichmann, N., Giardini, D., 2009. Earthquakes Induced by the Stimulation of an Enhanced  
1168 Geothermal System below Basel (Switzerland). *Seismological Research Letters* 80, 784–798.  
1169 <https://doi.org/10.1785/gssrl.80.5.784>
- 1170 Delvaux, D., 2001. Tectonic and palaeostress evolution of the Tanganyika-Rukwa-Malawi rift  
1171 segment, East African Rift System. In: Ziegler, P.A., Cavazza, W., Robertson, A.H.F.,  
1172 Crasquin-Soleau, S. (Eds.), *Peri-Tethys Memoir 6: Peri-Tethyan Rift/Wrench Basins and*  
1173 *Passive Margins*. 545–567.
- 1174 Delvaux, D., Barth, A., 2010. African stress pattern from formal inversion of focal mechanism  
1175 data. *Tectonophysics* 482, 105–128. <https://doi.org/10.1016/j.tecto.2009.05.009>
- 1176 Delvaux, D., Kervyn, F., Macheyeke, A.S., Temu, E.B., 2012. Geodynamic significance of the

- 1177 TRM segment in the East African Rift (W-Tanzania): Active tectonics and paleostress in the  
1178 Ufipa plateau and Rukwa basin. *Journal of Structural Geology* 37, 161–180.  
1179 <https://doi.org/10.1016/j.jsg.2012.01.008>
- 1180 Demurtas, M., Fondriest, M., Balsamo, F., Clemenzi, L., Storti, F., Bistacchi, A., Di Toro, G.,  
1181 2016. Structure of a normal seismogenic fault zone in carbonates: The Vado di Corno Fault,  
1182 Campo Imperatore, Central Apennines (Italy). *Journal of Structural Geology* 90, 185–206.  
1183 <https://doi.org/10.1016/j.jsg.2016.08.004>
- 1184 Deng, C., Fossen, H., Gawthorpe, R.L., Rotevatn, A., Jackson, C.A.L., Fazlikhani, H., 2017a.  
1185 Influence of fault reactivation during multiphase rifting: The Oseberg area, northern North  
1186 Sea rift. *Marine and Petroleum Geology* 86, 1252–1272.  
1187 <https://doi.org/10.1016/j.marpetgeo.2017.07.025>
- 1188 Deng, C., Gawthorpe, R.L., Finch, E., Fossen, H., 2017b. Influence of a pre-existing basement  
1189 weakness on normal fault growth during oblique extension: Insights from discrete element  
1190 modeling. *Journal of Structural Geology* 105, 44–61.  
1191 <https://doi.org/10.1016/j.jsg.2017.11.005>
- 1192 Dezayes, C., Genter, A., Valley, B., 2010. Overview of the Fracture Network at Different Scales  
1193 Within the Granite Reservoir of the EGS Soultz Site (Alsace, France). *Proceedings World*  
1194 *Geothermal Congress 2010*. Bali, Indonesia, 13.
- 1195 Diehl, T., Kraft, T., Kissling, E., Wiemer, S., 2017. The induced earthquake sequence related to  
1196 the St. Gallen deep geothermal project (Switzerland): Fault reactivation and fluid interactions  
1197 imaged by microseismicity. *Journal of Geophysical Research: Solid Earth* 122, 7272–7290.  
1198 <https://doi.org/10.1002/2017JB014473>

- 1199 Donath, F.A., 1962. Analysis of Basin-Range Structure, South-Central Oregon. GSA Bulletin 73,  
1200 1–16.
- 1201 Doré, A.G., Lundin, E.R., Fichler, C., Olesen, O., 1997. Patterns of basement structure and  
1202 reactivation along the NE Atlantic margin. *Journal of the Geological Society* 154, 85–92.
- 1203 Duffy, O.B., Bell, R.E., Jackson, C.A.L., Gawthorpe, R.L., Whipp, P.S., 2015. Fault growth and  
1204 interactions in a multiphase rift fault network: Horda Platform, Norwegian North Sea. *Journal*  
1205 *of Structural Geology* 80, 99–119. <https://doi.org/10.1016/j.jsg.2015.08.015>
- 1206 Dunbar, J.A., Sawyer, D.S., 1989. How preexisting weaknesses control the style of continental  
1207 breakup. *Journal of Geophysical Research* 94, 7278–7292.  
1208 <https://doi.org/10.1029/JB094iB06p07278>
- 1209 Ebinger, C., 2005. Continental break-up: The East African perspective. *Astronomy and*  
1210 *Geophysics* 46, 2.16--2.21. <https://doi.org/10.1111/j.1468-4004.2005.46216.x>
- 1211 Ebinger, C.J., 1989. Tectonic development of the western branch of the East African rift system.,  
1212 *Geological Society of America Bulletin*. [https://doi.org/10.1130/0016-](https://doi.org/10.1130/0016-7606(1989)101<0885:TDOTWB>2.3.CO;2)  
1213 [7606\(1989\)101<0885:TDOTWB>2.3.CO;2](https://doi.org/10.1130/0016-7606(1989)101<0885:TDOTWB>2.3.CO;2)
- 1214 Ebinger, C.J., Rosendahl, B.R., Reynolds, D.J., 1987. Tectonic model of the Malaŵi rift, Africa.  
1215 *Tectonophysics* 141, 215–235. [https://doi.org/10.1016/0040-1951\(87\)90187-9](https://doi.org/10.1016/0040-1951(87)90187-9)
- 1216 Etheridge, M.A., 1986. On the reactivation of extensional fault systems. *Philosophical*  
1217 *Transactions - Royal Society of London, Series A* 317, 179–194.  
1218 <https://doi.org/10.1098/rsta.1986.0031>
- 1219 Færseth, R.B., Gabrielsen, R.H., Hurich, C.A., 1995. Influence of basement in structuring of the



- 1220 North Sea Basin, offshore southwest Norway. *Norsk Geologisk Tidsskrift* 75, 105–119.
- 1221 Fairhead, J.D., Henderson, N.B., 1977. The seismicity of southern Africa and incipient rifting.  
1222 *Tectonophysics* 41, T19–T26. [https://doi.org/10.1016/0040-1951\(77\)90133-0](https://doi.org/10.1016/0040-1951(77)90133-0)
- 1223 Fazlikhani, H., Fossen, H., Gawthorpe, R.L., Faleide, J.I., Bell, R.E., 2017. Basement structure  
1224 and its influence on the structural configuration of the northern North Sea rift. *Tectonics* 36,  
1225 1151–1177. <https://doi.org/10.1002/2017TC004514>
- 1226 Fonseca, J., 1988. The Sou Hills: A barrier to faulting in the central Nevada Seismic Belt. *Journal*  
1227 *of Geophysical Research: Solid Earth* 93, 475–489.  
1228 <https://doi.org/10.1029/JB093iB01p00475>
- 1229 Fossen, H., Gabrielsen, R.H., Faleide, J.I., Hurich, C.A., 2014. Crustal stretching in the  
1230 Scandinavian Caledonides as revealed by deep seismic data. *Geology* 42, 791–794.  
1231 <https://doi.org/10.1130/G35842.1>
- 1232 Fossen, H., Hurich, C.A., 2005. The Hardangerfjord Shear Zone in SW Norway and the North Sea:  
1233 A large-scale low-angle shear zone in the Caledonian crust. *Journal of the Geological Society*  
1234 162, 675–687. <https://doi.org/10.1144/0016-764904-136>
- 1235 Fossen, H., Khani, H.F., Faleide, J.I., Ksienzyk, A.K., Dunlap, W.J., 2016. Post-Caledonian  
1236 extension in the West Norway-northern North Sea region: the role of structural inheritance.  
1237 Geological Society, London, Special Publications. <https://doi.org/10.1144/SP439.6>
- 1238 Fossen, H., Rotevatn, A., 2016. Fault linkage and relay structures in extensional settings-A review.  
1239 *Earth-Science Reviews* 154, 14–28. <https://doi.org/10.1016/j.earscirev.2015.11.014>
- 1240 Ghosh, N., Hatui, K., Chattopadhyay, A., 2020. Evolution of fault patterns within a zone of pre-

- 1241 existing pervasive anisotropy during two successive phases of extensions: an experimental  
1242 study. *Geo-Marine Letters* 40, 53–74. <https://doi.org/10.1007/s00367-019-00627-6>
- 1243 Giba, M., Walsh, J.J., Nicol, A., 2012. Segmentation and growth of an obliquely reactivated  
1244 normal fault. *Journal of Structural Geology* 39, 253–267.  
1245 <https://doi.org/10.1016/j.jsg.2012.01.004>
- 1246 Gibson, G.M., Meixner, A.J., Withnall, I.W., Korsch, R.J., Hutton, L.J., Jones, L.E.A., Holzschuh,  
1247 J., Costelloe, R.D., Henson, P.A., Saygin, E., 2016. Basin architecture and evolution in the  
1248 Mount Isa mineral province, northern Australia: Constraints from deep seismic reflection  
1249 profiling and implications for ore genesis. *Ore Geology Reviews* 76, 414–441.  
1250 <https://doi.org/10.1016/j.oregeorev.2015.07.013>
- 1251 Gibson, G.M., Totterdell, J.M., White, L.T., Mitchell, C.H., Stacey, A.R., Morse, M.P., Whitaker,  
1252 A., 2013. Pre-existing basement structure and its influence on continental rifting and fracture  
1253 zone development along Australia’s southern rifted margin. *Journal of the Geological Society*  
1254 170, 365–377. <https://doi.org/10.1144/jgs2012-040>
- 1255 Glaas, C., Vidal, J., Genter, A., 2021. Structural characterization of naturally fractured geothermal  
1256 reservoirs in the central Upper Rhine Graben. *Journal of Structural Geology* 148, 104370.  
1257 <https://doi.org/10.1016/j.jsg.2021.104370>
- 1258 Gleeson, S.A., Dyardley, B.W., Munz, I.A., Boyce, A.J., 2003. Infiltration of basinal fluids into  
1259 high-grade basement, South Norway: Sources and behaviour of waters and brines. *Geofluids*  
1260 3, 33–48. <https://doi.org/10.1046/j.1468-8123.2003.00047.x>
- 1261 Global Volcanism Project, 2013. *Volcanoes of the World*, v. 4.10.3 (15 Oct 2021).  
1262 <https://doi.org/https://doi.org/10.5479/si.GVP.VOTW4-2013>

- 1263 Gouiza, M., Naliboff, J., 2021. Rheological inheritance controls the formation of segmented rifted  
1264 margins in cratonic lithosphere. *Nature Communications* 12, 1–9.  
1265 <https://doi.org/10.1038/s41467-021-24945-5>
- 1266 Gouiza, M., Paton, D.A., 2019. The Role of Inherited Lithospheric Heterogeneities in Defining  
1267 the Crustal Architecture of Rifted Margins and the Magmatic Budget During Continental  
1268 Breakup. *Geochemistry, Geophysics, Geosystems* 20, 1836–1853.  
1269 <https://doi.org/10.1029/2018GC007808>
- 1270 Haimson, B., 2006. True Triaxial Stresses and the Brittle Fracture of Rock. In: Dresen, G., Zang,  
1271 A., Stephansson, O. (Eds.), *Rock Damage and Fluid Transport, Part I*. Birkhäuser Basel,  
1272 Basel, 1101–1130. [https://doi.org/10.1007/3-7643-7712-7\\_12](https://doi.org/10.1007/3-7643-7712-7_12)
- 1273 Handy, M.R., Hirth, G., Bürgmann, R., 2007. Continental Fault Structure and Rheology from the  
1274 Frictional-to-Viscous Transition Downward. In: Handy, M.R., Hirth, G., Hovius, N. (Eds.),  
1275 *Tectonic Faults: Agents of Change on a Dynamic Earth*. The MIT Press.  
1276 <https://doi.org/10.7551/mitpress/6703.003.0008>
- 1277 Healy, D., 2009. Anisotropy, pore fluid pressure and low angle normal faults. *Journal of Structural*  
1278 *Geology* 31, 561–574. <https://doi.org/10.1016/j.jsg.2009.03.001>
- 1279 Hecker, S., DeLong, S.B., Schwartz, D.P., 2021. Rapid strain release on the Bear River fault zone,  
1280 Utah–Wyoming—The impact of preexisting structure on the rupture behavior of a new  
1281 normal fault. *Tectonophysics* 808, 228819. <https://doi.org/10.1016/j.tecto.2021.228819>
- 1282 Heilman, E., Kolawole, F., Atekwana, E.A., Mayle, M., 2019. Controls of Basement Fabric on the  
1283 Linkage of Rift Segments. *Tectonics* 38, 1337–1366. <https://doi.org/10.1029/2018TC005362>

- 1284 Heron, P.J., Peace, A.L., McCaffrey, K., Welford, J.K., Wilson, R., Hunen, J., Pysklywec, R.N.,  
1285 2019. Segmentation of rifts through structural inheritance: Creation of the Davis Strait.  
1286 *Tectonics* 2019TC005578. <https://doi.org/10.1029/2019TC005578>
- 1287 Hodge, M., Biggs, J., Fagereng, Å., Mdala, H., Wedmore, L.N.J., Williams, J.N., 2020. Evidence  
1288 From High-Resolution Topography for Multiple Earthquakes on High Slip-to-Length Fault  
1289 Scarps: The Bilila-Mtakataka Fault, Malawi. *Tectonics* 39, 1–24.  
1290 <https://doi.org/10.1029/2019TC005933>
- 1291 Hodge, M., Fagereng, Å., Biggs, J., Mdala, H., 2018. Controls on Early-Rift Geometry: New  
1292 Perspectives From the Bilila-Mtakataka Fault, Malawi. *Geophysical Research Letters* 45,  
1293 3896–3905. <https://doi.org/10.1029/2018GL077343>
- 1294 Hoggard, M.J., Czarnota, K., Richards, F.D., Huston, D.L., Jaques, A.L., Ghelichkhan, S., 2020.  
1295 Global distribution of sediment-hosted metals controlled by craton edge stability. *Nature*  
1296 *Geoscience* 13, 504–510. <https://doi.org/10.1038/s41561-020-0593-2>
- 1297 Holdsworth, R.E., 2004. Weak Faults--Rotten Cores. *Science* 303, 181–182.  
1298 <https://doi.org/10.1126/science.1092491>
- 1299 Holdsworth, R.E., Butler, C.A., Roberts, A.M., 1997. The recognition of reactivation during  
1300 continental deformation. *Journal of the Geological Society* 154, 73–78.  
1301 <https://doi.org/10.1144/gsjgs.154.1.0073>
- 1302 Holdsworth, R.E., Handa, M., Miller, J.A., Buick, I.S., 2001a. Continental reactivation and  
1303 reworking: an introduction. Geological Society, London, Special Publications 184, 1–12.  
1304 <https://doi.org/10.1144/GSL.SP.2001.184.01.01>

- 1305 Holdsworth, R.E., Selby, D., Dempsey, E., Scott, L., Hardman, K., Fallick, A.E., Bullock, R.,  
1306 2020. The nature and age of Mesoproterozoic strike-slip faulting based on Re–Os  
1307 geochronology of syntectonic copper mineralization, Assynt Terrane, NW Scotland. *Journal*  
1308 *of the Geological Society* 177, 686–699. <https://doi.org/10.1144/jgs2020-011>
- 1309 Holdsworth, R.E., Stewart, M., Imber, J., Strachan, R.A., 2001b. The structure and rheological  
1310 evolution of reactivated continental fault zones: a review and case study. Geological Society,  
1311 London, Special Publications 184, 115–137. <https://doi.org/10.1144/GSL.SP.2001.184.01.07>
- 1312 Hubbert, M.K., 1951. Mechanical basis for certain familiar geologic structures. *Bulletin of the*  
1313 *Geological Society of America* 62, 355–372. [https://doi.org/10.1130/0016-](https://doi.org/10.1130/0016-7606(1951)62[355:MBFCFG]2.0.CO;2)  
1314 [7606\(1951\)62\[355:MBFCFG\]2.0.CO;2](https://doi.org/10.1130/0016-7606(1951)62[355:MBFCFG]2.0.CO;2)
- 1315 Jackson, C.A.L., Rotevatn, A., 2013. 3D seismic analysis of the structure and evolution of a salt-  
1316 influenced normal fault zone: A test of competing fault growth models. *Journal of Structural*  
1317 *Geology* 54, 215–234. <https://doi.org/10.1016/j.jsg.2013.06.012>
- 1318 Jackson, J., Blenkinsop, T., 1997. The Bilila-Mtakataka fault in Malawi: an active, 100-km long,  
1319 normal fault segment in thick seismogenic crust. *Tectonics* 16, 137–150.  
1320 <https://doi.org/10.1029/96TC02494>
- 1321 Jaeger, J.C., Cook, N.G.W., 1979. *Fundamentals of Rock Mechanics*, 3rd ed. Chapman and Hall,  
1322 London.
- 1323 Katumwehe, A.B., Abdelsalam, M.G., Atekwana, E.A., 2015. The role of pre-existing  
1324 Precambrian structures in rift evolution: The Albertine and Rhino grabens, Uganda.  
1325 *Tectonophysics* 646, 117–129. <https://doi.org/10.1016/j.tecto.2015.01.022>

- 1326 Keep, M., McClay, K.R., 1997. Analogue modelling of multiphase rift systems. *Tectonophysics*  
1327 273, 239–270. [https://doi.org/10.1016/S0040-1951\(96\)00272-7](https://doi.org/10.1016/S0040-1951(96)00272-7)
- 1328 Kinabo, B.D., Atekwana, E.A., Hogan, J.P., Modisi, M.P., Wheaton, D.D., Kampunzu, A.B., 2007.  
1329 Early structural development of the Okavango rift zone, NW Botswana. *Journal of African*  
1330 *Earth Sciences* 48, 125–136. <https://doi.org/10.1016/j.jafrearsci.2007.02.005>
- 1331 Kirkpatrick, J.D., Bezerra, F.H.R., Shipton, Z.K., Do Nascimento, A.F., Pytharouli, S.I., Lunn,  
1332 R.J., Soden, A.M., 2013. Scale-dependent influence of pre-existing basement shear zones on  
1333 rift faulting: a case study from NE Brazil. *Journal of the Geological Society* 170, 237–247.  
1334 <https://doi.org/10.1144/jgs2012-043>
- 1335 Kolawole, F., Atekwana, E.A., Laó-Dávila, D.A., Abdelsalam, M.G., Chindandali, P.R., Salima,  
1336 J., Kalindekafe, L., 2018. Active Deformation of Malawi Rift’s North Basin Hinge Zone  
1337 Modulated by Reactivation of Preexisting Precambrian Shear Zone Fabric. *Tectonics* 37,  
1338 683–704. <https://doi.org/10.1002/2017TC004628>
- 1339 Kolawole, F., Firkins, M.C., Al Wahaibi, T.S., Atekwana, E.A., Soreghan, M.J., 2021a. Rift  
1340 interaction zones and the stages of rift linkage in active segmented continental rift systems.  
1341 *Basin Research* 33, 2984–3020. <https://doi.org/10.1111/bre.12592>
- 1342 Kolawole, F., Phillips, T.B., Atekwana, E.A., Jackson, C.A.L., 2021b. Structural Inheritance  
1343 Controls Strain Distribution During Early Continental Rifting, Rukwa Rift. *Frontiers in Earth*  
1344 *Science* 9, 1–14. <https://doi.org/10.3389/feart.2021.707869>
- 1345 Krabbendam, M., Barr, T.D., 2000. Proterozoic orogens and the break-up of Gondwana: Why did  
1346 some orogens not rift? *Journal of African Earth Sciences* 31, 35–49.  
1347 [https://doi.org/10.1016/S0899-5362\(00\)00071-3](https://doi.org/10.1016/S0899-5362(00)00071-3)

- 1348 Kuszniir, N.J., Park, R.G., 1986. Continental lithosphere strength: The critical role of lower crustal  
1349 deformation. *Geological Society Special Publication* 24, 79–93.  
1350 <https://doi.org/10.1144/GSL.SP.1986.024.01.09>
- 1351 Laó-Dávila, D.A., Al-Salmi, H.S., Abdelsalam, M.G., Atekwana, E.A., 2015. Hierarchical  
1352 segmentation of the Malawi Rift: The influence of inherited lithospheric heterogeneity and  
1353 kinematics in the evolution of continental rifts. *Tectonics* 34, 2399–2417.  
1354 <https://doi.org/10.1002/2015TC003953>
- 1355 Leclère, H., Fabbri, O., 2013. A new three-dimensional method of fault reactivation analysis.  
1356 *Journal of Structural Geology* 48, 153–161. <https://doi.org/10.1016/j.jsg.2012.11.004>
- 1357 Lisle, R.J., Srivastava, D.C., 2004. Test of the frictional reactivation theory for faults and validity  
1358 of fault-slip analysis. *Geology* 32, 569–572. <https://doi.org/10.1130/G20408.1>
- 1359 Lyon, P.J., Boulton, P.J., Hillis, R.R., Bierbrauer, K., 2007. Basement controls on fault development  
1360 in the Penola Trough, Otway Basin, and implications for fault-bounded hydrocarbon traps.  
1361 *Australian Journal of Earth Sciences* 54, 675–689.  
1362 <https://doi.org/10.1080/08120090701305228>
- 1363 Macgregor, D., 2015. History of the development of the East African Rift System: A series of  
1364 interpreted maps through time. *Journal of African Earth Sciences* 101, 232–252.  
1365 <https://doi.org/10.1016/j.jafrearsci.2014.09.016>
- 1366 Manatschal, G., Lavie, L., Chenin, P., 2015. The role of inheritance in structuring hyperextended  
1367 rift systems: Some considerations based on observations and numerical modeling. *Gondwana*  
1368 *Research* 27, 140–164. <https://doi.org/10.1016/j.gr.2014.08.006>

- 1369 Mandl, G., Jong, L.N.J., Maltha, A., 1977. Shear zones in granular material. *Rock Mechanics* 9,  
1370 95–144. <https://doi.org/10.1007/BF01237876>
- 1371 Massironi, M., Bistacchi, A., Menegon, L., 2011. Misoriented faults in exhumed metamorphic  
1372 complexes: Rule or exception? *Earth and Planetary Science Letters* 307, 233–239.  
1373 <https://doi.org/10.1016/j.epsl.2011.04.041>
- 1374 McCaffrey, K.J.W., 1997. Controls on reactivation of a major fault zone: the Fair Head–Clew Bay  
1375 line in Ireland. *Journal of the Geological Society* 154, 129–133.  
1376 <https://doi.org/10.1144/gsjgs.154.1.0129>
- 1377 McConnell, R.B., 1972. Geological Development of the Rift System of Eastern Africa. *GSA*  
1378 *Bulletin* 2549–2572.
- 1379 McHarg, S., Elders, C., Cunneen, J., 2019. Normal fault linkage and reactivation, Dampier Sub-  
1380 basin, Western Australia. *Australian Journal of Earth Sciences* 66, 209–225.  
1381 <https://doi.org/10.1080/08120099.2019.1519848>
- 1382 Milicich, S.D., Mortimer, N., Villamor, P., Wilson, C.J.N., Chambefort, I., Sagar, M.W., Ireland,  
1383 T.R., 2021. The Mesozoic terrane boundary beneath the Taupo Volcanic Zone, New Zealand,  
1384 and potential controls on geothermal system characteristics. *New Zealand Journal of Geology*  
1385 *and Geophysics* 64, 518–529. <https://doi.org/10.1080/00288306.2020.1823434>
- 1386 Miller, J.M.L., Norvick, M.S., Wilson, C.J.L., 2002. Basement controls on rifting and the  
1387 associated formation of ocean transform faults - Cretaceous continental extension of the  
1388 southern margin of Australia. *Tectonophysics* 359, 131–155. <https://doi.org/10.1016/S0040->  
1389 [1951\(02\)00508-5](https://doi.org/10.1016/S0040-1951(02)00508-5)



- 1390 Molnar, N., Cruden, A., Betts, P., 2020. The role of inherited crustal and lithospheric architecture  
1391 during the evolution of the Red Sea: Insights from three dimensional analogue experiments.  
1392 Earth and Planetary Science Letters 544, 116377. <https://doi.org/10.1016/j.epsl.2020.116377>
- 1393 Molnar, N.E., Cruden, A.R., Betts, P.G., 2017. Interactions between propagating rotational rifts  
1394 and linear rheological heterogeneities: Insights from three-dimensional laboratory  
1395 experiments. *Tectonics* 36, 420–443. <https://doi.org/10.1002/2016TC004447>
- 1396 Moore, D.E., Lockner, D.A., 2004. Crystallographic controls on the frictional behavior of dry and  
1397 water-saturated sheet structure minerals. *Journal of Geophysical Research* 109, B03401.  
1398 <https://doi.org/10.1029/2003JB002582>
- 1399 Morley, C.K., 2010. Stress re-orientation along zones of weak fabrics in rifts: An explanation for  
1400 pure extension in “oblique” rift segments? *Earth and Planetary Science Letters* 297, 667–673.  
1401 <https://doi.org/10.1016/j.epsl.2010.07.022>
- 1402 Morley, C.K., 1995. Developments in the structural geology of rifts over the last decade and their  
1403 impact on hydrocarbon exploration. *Hydrocarbon Habitat in Rift Basins* 1–32.
- 1404 Morley, C.K., Haranya, C., Phoosongsee, W., Pongwapee, S., Kornawan, A., Wonganan, N.,  
1405 2004. Activation of rift oblique and rift parallel pre-existing fabrics during extension and their  
1406 effect on deformation style: examples from the rifts of Thailand. *Journal of Structural*  
1407 *Geology* 26, 1803–1829. <https://doi.org/10.1016/j.jsg.2004.02.014>
- 1408 Morris, A., Ferrill, D.A., Henderson, D.B., 1996. Slip-tendency analysis and fault reactivation.  
1409 *Geology* 24, 275–278. [https://doi.org/10.1130/0091-](https://doi.org/10.1130/0091-7613(1996)024<0275:STAAFR>2.3.CO;2)  
1410 [7613\(1996\)024<0275:STAAFR>2.3.CO;2](https://doi.org/10.1130/0091-7613(1996)024<0275:STAAFR>2.3.CO;2)

- 1411 Mortimer, N., 2004. New Zealand's geological foundations. *Gondwana Research* 7, 261–272.  
1412 [https://doi.org/10.1016/S1342-937X\(05\)70324-5](https://doi.org/10.1016/S1342-937X(05)70324-5)
- 1413 Mortimer, N., Davey, F.J., Melhuish, A., Yu, J., Godfrey, N.J., 2002. Geological interpretation of  
1414 a deep seismic reflection profile across the Eastern Province and Median Batholith, New  
1415 Zealand: Crustal architecture of an extended Phanerozoic convergent orogen. *New Zealand  
1416 Journal of Geology and Geophysics* 45, 349–363.  
1417 <https://doi.org/10.1080/00288306.2002.9514978>
- 1418 Muir, R.J., Bradshaw, J.D., Weaver, S.D., Laird, M.G., 2000. The influence of basement structure  
1419 on the evolution of the Taranaki Basin, New Zealand. *Journal of the Geological Society* 157,  
1420 1179–1185. <https://doi.org/10.1144/jgs.157.6.1179>
- 1421 Muirhead, J.D., Kattenhorn, S.A., 2018. Activation of preexisting transverse structures in an  
1422 evolving magmatic rift in East Africa. *Journal of Structural Geology* 106, 1–18.  
1423 <https://doi.org/10.1016/j.jsg.2017.11.004>
- 1424 Muirhead, J.D., Wright, L.J.M., Scholz, C.A., 2019. Rift evolution in regions of low magma input  
1425 in East Africa. *Earth and Planetary Science Letters* 506, 332–346.  
1426 <https://doi.org/10.1016/j.epsl.2018.11.004>
- 1427 Murrell, S.A.F., 1963. A criterion for brittle fracture of rocks and concrete under triaxial stress and  
1428 the effect of pore pressure on the criterion. In: Fairhurst, C. (Ed.), *Proceedings of the 5th  
1429 Symposium on Rock Mechanics*. Minneapolis, Minnesota, 563–577.
- 1430 Norini, G., Carrasco-Núñez, G., Corbo-Camargo, F., Lermo, J., Rojas, J.H., Castro, C., Bonini,  
1431 M., Montanari, D., Corti, G., Moratti, G., Piccardi, L., Chavez, G., Zuluaga, M.C., Ramirez,  
1432 M., Cedillo, F., 2019. The structural architecture of the Los Humeros volcanic complex and

- 1433 geothermal field. *Journal of Volcanology and Geothermal Research* 381, 312–329.  
1434 <https://doi.org/10.1016/j.jvolgeores.2019.06.010>
- 1435 Numelin, T.J., Marone, C., Kirby, E., 2007. Frictional properties of natural fault gouge from a low-  
1436 angle normal fault, Panamit Valley, California. *Tectonics* 26, 1–14.  
1437 <https://doi.org/10.1029/2005TC001916>
- 1438 Nutz, A., Ragon, T., Schuster, M., 2022. Cenozoic tectono-sedimentary evolution of the northern  
1439 Turkana Depression (East African Rift System) and its significance for continental rifts. *Earth  
1440 and Planetary Science Letters* 578, 117285. <https://doi.org/10.1016/j.epsl.2021.117285>
- 1441 Nyblade, A.A., Brazier, R.A., 2002. Precambrian lithospheric controls on the development of the  
1442 East African rift system. *Geology* 30, 755–758. [https://doi.org/10.1130/0091-  
1443 7613\(2002\)030<0755:PLCOTD>2.0.CO;2](https://doi.org/10.1130/0091-7613(2002)030<0755:PLCOTD>2.0.CO;2)
- 1444 Ojo, O.O., Ohenhen, L.O., Kolawole, F., Johnson, S.G., Chindandali, P.R., Atekwana, E.A., Laó-  
1445 Dávila, D.A., 2022. Under-Displaced Normal Faults: Strain Accommodation Along an Early-  
1446 Stage Rift-Bounding Fault in the Southern Malawi Rift. *Frontiers in Earth Science* 10, 1–19.  
1447 <https://doi.org/10.3389/feart.2022.846389>
- 1448 Osagiede, E.E., Rosenau, M., Rotevatn, A., Gawthorpe, R., Jackson, C.A.L., Rudolf, M., 2021.  
1449 Influence of Zones of Pre-Existing Crustal Weakness on Strain Localization and Partitioning  
1450 During Rifting: Insights From Analog Modeling Using High-Resolution 3D Digital Image  
1451 Correlation. *Tectonics* 40, 1–30. <https://doi.org/10.1029/2021TC006970>
- 1452 Osagiede, E.E., Rotevatn, A., Gawthorpe, R., Kristensen, T.B., Jackson, C.A.L., Marsh, N., 2020.  
1453 Pre-existing intra-basement shear zones influence growth and geometry of non-colinear  
1454 normal faults, western Utsira High–Heimdal Terrace, North Sea. *Journal of Structural*

- 1455 Geology 130, 103908. <https://doi.org/10.1016/j.jsg.2019.103908>
- 1456 Paton, D.A., 2006. Influence of crustal heterogeneity on normal fault dimensions and evolution:  
1457 southern South Africa extensional system. *Journal of Structural Geology* 28, 868–886.  
1458 <https://doi.org/10.1016/j.jsg.2006.01.006>
- 1459 Peace, A., Dempsey, E., Schiffer, C., Welford, J., McCaffrey, K., Imber, J., Phethean, J., 2018a.  
1460 Evidence for Basement Reactivation during the Opening of the Labrador Sea from the  
1461 Makkovik Province, Labrador, Canada: Insights from Field Data and Numerical Models.  
1462 *Geosciences* 8, 308. <https://doi.org/10.3390/geosciences8080308>
- 1463 Peace, A., McCaffrey, K., Imber, J., van Hunen, J., Hobbs, R., Wilson, R., 2018b. The role of pre-  
1464 existing structures during rifting, continental breakup and transform system development,  
1465 offshore West Greenland. *Basin Research* 30, 373–394. <https://doi.org/10.1111/bre.12257>
- 1466 Petersen, K.D., Schiffer, C., 2016. Wilson cycle passive margins: Control of orogenic inheritance  
1467 on continental breakup. *Gondwana Research* 39, 131–144.  
1468 <https://doi.org/10.1016/j.gr.2016.06.012>
- 1469 Petit, C., Déverchère, J., Houdry, F., Sankov, V.A., Melnikova, V.I., Delvaux, D., 1996. Present-  
1470 day stress field changes along the Baikal rift and tectonic implications. *Tectonics* 15, 1171–  
1471 1191. <https://doi.org/10.1029/96TC00624>
- 1472 Philippon, M., Willingshofer, E., Sokoutis, D., Corti, G., Sani, F., Bonini, M., Cloetingh, S., 2015.  
1473 Slip re-orientation in oblique rifts. *Geology* 43, 147–150. <https://doi.org/10.1130/G36208.1>
- 1474 Phillips, T.B., Jackson, C.A.L., Bell, R.E., Duffy, O.B., Fossen, H., 2016. Reactivation of  
1475 intrabasement structures during rifting: A case study from offshore southern Norway. *Journal*

- 1476 of Structural Geology 91, 54–73. <https://doi.org/10.1016/j.jsg.2016.08.008>
- 1477 Phillips, T.B., Mccaffrey, K., Magarinos, L., 2021a. Coupling between shallow and deep fault  
1478 populations governs along-strike variations in fault reactivation and structural inheritance, the  
1479 Laminaria High, NW Shelf of Australia. Preprint.  
1480 <https://doi.org/https://doi.org/10.31223/X5G32J>
- 1481 Phillips, T.B., McCaffrey, K.J.W., 2019. Terrane Boundary Reactivation, Barriers to Lateral Fault  
1482 Propagation and Reactivated Fabrics: Rifting Across the Median Batholith Zone, Great South  
1483 Basin, New Zealand. *Tectonics* 38, 4027–4053. <https://doi.org/10.1029/2019TC005772>
- 1484 Phillips, T.B., Naliboff, J.B., Mccaffrey, K.J.W., Pan, S., van Hunen, J., 2021b. The influence of  
1485 crustal strength on rift geometry and development - Insights from 3D numerical modelling.  
1486 Preprint.
- 1487 Piqué, A., Laville, E., 1996. The Central Atlantic rifting: Reactivation of palaeozoic structures?  
1488 *Journal of Geodynamics* 21, 235–255. [https://doi.org/10.1016/0264-3707\(95\)00022-4](https://doi.org/10.1016/0264-3707(95)00022-4)
- 1489 Poggi, V., Durrheim, R., Tuluka, G.M., Weatherill, G., Gee, R., Pagani, M., Nyblade, A., Delvaux,  
1490 D., 2017. Assessing seismic hazard of the East African Rift: a pilot study from GEM and  
1491 AfricaArray. *Bulletin of Earthquake Engineering* 15, 4499–4529.  
1492 <https://doi.org/10.1007/s10518-017-0152-4>
- 1493 Ranalli, G., Yin, Z.M., 1990. Critical stress difference and orientation of faults in rocks with  
1494 strength anisotropies: the two-dimensional case. *Journal of Structural Geology* 12, 1067–  
1495 1071. [https://doi.org/10.1016/0191-8141\(90\)90102-5](https://doi.org/10.1016/0191-8141(90)90102-5)
- 1496 Reeve, M.T., Bell, R.E., Duffy, O.B., Jackson, C.A.L., Sansom, E., 2015. The growth of non-

- 1497 colinear normal fault systems; What can we learn from 3D seismic reflection data? *Journal*  
1498 *of Structural Geology* 70, 141–155. <https://doi.org/10.1016/j.jsg.2014.11.007>
- 1499 Riller, U., Clark, M.D., Daxberger, H., Doman, D., Lenauer, I., Plath, S., Santimano, T., 2017.  
1500 Fault-slip inversions: Their importance in terms of strain, heterogeneity, and kinematics of  
1501 brittle deformation. *Journal of Structural Geology* 101, B2–B6.  
1502 <https://doi.org/10.1016/j.jsg.2017.06.013>
- 1503 Ring, U., 1994. The influence of preexisting structure on the evolution of the Cenozoic Malawi  
1504 rift (East African rift system). *Tectonics* 13, 313–326. <https://doi.org/10.1029/93TC03188>
- 1505 Robertson, E.A.M., Biggs, J., Cashman, K. V, Floyd, M.A., Vye-Brown, C., 2016. Influence of  
1506 regional tectonics and pre-existing structures on the formation of elliptical calderas in the  
1507 Kenyan Rift. *Geological Society Special Publication*. 43–67.  
1508 <https://doi.org/10.1144/SP420.12>
- 1509 Roche, V., Childs, C., Madritsch, H., Camanni, G., 2020. Layering and structural inheritance  
1510 controls on fault zone structure in three dimensions: A case study from the northern Molasse  
1511 basin, Switzerland. *Journal of the Geological Society* 177, 493–508.  
1512 <https://doi.org/10.1144/jgs2019-052>
- 1513 Rotevatn, A., Jackson, C.A.L., Tvedt, A.B.M., Bell, R.E., Blækkan, I., 2019. How do normal faults  
1514 grow? *Journal of Structural Geology* 125, 174–184. <https://doi.org/10.1016/j.jsg.2018.08.005>
- 1515 Rotevatn, A., Kristensen, T.B., Ksienzyk, A.K., Wemmer, K., Henstra, G.A., Midtkandal, I.,  
1516 Grundvåg, S.A., Andresen, A., 2018. Structural inheritance and rapid rift-length  
1517 establishment in a multiphase rift: the East Greenland rift system and its Caledonian orogenic  
1518 ancestry. *Tectonics* 37, 1858–1875. <https://doi.org/10.1029/2018TC005018>

- 1519 Rotevatn, A, Kristensen, T.B., Ksienzyk, A.K., Wemmer, K., Henstra, G.A., Midtkandal, I.,  
1520 Grundvåg, S.A., Andresen, A., 2018. Structural Inheritance and Rapid Rift-Length  
1521 Establishment in a Multiphase Rift: The East Greenland Rift System and its Caledonian  
1522 Orogenic Ancestry. *Tectonics* 37, 1858–1875. <https://doi.org/10.1029/2018TC005018>
- 1523 Rowland, J. V., Sibson, R.H., 2004. Structural controls on hydrothermal flow in a segmented rift  
1524 system, Taupo Volcanic Zone, New Zealand. *Geofluids* 4, 259–283.  
1525 <https://doi.org/10.1111/j.1468-8123.2004.00091.x>
- 1526 Rowland, J. V., Simmons, S.F., 2012. Hydrologic, magmatic, and tectonic controls on  
1527 hydrothermal flow, Taupo Volcanic Zone, New Zealand: Implications for the formation of  
1528 epithermal vein deposits. *Economic Geology* 107, 427–457.  
1529 <https://doi.org/10.2113/econgeo.107.3.427>
- 1530 Saalman, K., Mänttari, I., Nyakecho, C., Isabirye, E., 2016. Age, tectonic evolution and origin of  
1531 the Aswa Shear Zone in Uganda: Activation of an oblique ramp during convergence in the  
1532 East African Orogen. *Journal of African Earth Sciences* 117, 303–330.  
1533 <https://doi.org/10.1016/j.jafrearsci.2016.02.002>
- 1534 Samsu, A., Cruden, A.R., Hall, M., Micklethwaite, S., Denyszyn, S.W., 2019. The influence of  
1535 basement faults on local extension directions: Insights from potential field geophysics and  
1536 field observations. *Basin Research* 31, 782–807. <https://doi.org/10.1111/bre.12344>
- 1537 Samsu, A., Cruden, A.R., Micklethwaite, S., Grose, L., Vollgger, S.A., 2020. Scale matters: The  
1538 influence of structural inheritance on fracture patterns. *Journal of Structural Geology* 130,  
1539 103896. <https://doi.org/10.1016/j.jsg.2019.103896>
- 1540 Samsu, A., Cruden, A.R., Molnar, N.E., Weinberg, R.F., 2021. Inheritance of penetrative basement

- 1541 anisotropies by extension-oblique faults: Insights from analogue experiments. *Tectonics* 1–  
1542 19. <https://doi.org/10.1029/2020tc006596>
- 1543 Sandwell, D., Mellors, R., Tong, X., Wei, M., Wessel, P., 2011. Open radar interferometry  
1544 software for mapping surface Deformation. *Eos, Transactions American Geophysical Union*.  
1545 <https://doi.org/10.1029/2011EO280002>
- 1546 Schellart, W.P., 2000. Shear test results for cohesion and friction coefficients for different granular  
1547 materials: Scaling implications for their usage in analogue modelling. *Tectonophysics* 324,  
1548 1–16. [https://doi.org/10.1016/S0040-1951\(00\)00111-6](https://doi.org/10.1016/S0040-1951(00)00111-6)
- 1549 Schiffer, C., Doré, A.G., Foulger, G.R., Franke, D., Geoffroy, L., Gernigon, L., Holdsworth, B.,  
1550 Kuszniir, N., Lundin, E., McCaffrey, K., Peace, A.L., Petersen, K.D., Phillips, T.B.,  
1551 Stephenson, R., Stoker, M.S., Welford, J.K., 2020. Structural inheritance in the North  
1552 Atlantic. *Earth-Science Reviews* 206, 102975.  
1553 <https://doi.org/10.1016/j.earscirev.2019.102975>
- 1554 Schiffer, C., Peace, A., Phethean, J., Gernigon, L., McCaffrey, K., Petersen, K.D., Foulger, G.,  
1555 2018. The Jan Mayen microplate complex and the Wilson cycle. Geological Society, London,  
1556 Special Publications 470. <https://doi.org/10.1144/SP470.2>
- 1557 Scholz, C.A., Shillington, D.J., Wright, L.J.M., Accardo, N., Gaherty, J.B., Chindandali, P., 2020.  
1558 Intrarift fault fabric, segmentation, and basin evolution of the Lake Malawi (Nyasa) Rift, East  
1559 Africa. *Geosphere* 16, 1293–1311. <https://doi.org/10.1130/GES02228.1>
- 1560 Schumacher, M.E., 2002. Upper Rhine Graben: Role of preexisting structures during rift evolution.  
1561 *Tectonics* 21, 6-1-6–17. <https://doi.org/10.1029/2001TC900022>



- 1562 Shea, W.T., Kronenberg, A.K., 1993. Strength and anisotropy of foliated rocks with varied mica  
1563 contents. *Journal of Structural Geology* 15, 1097–1121. <https://doi.org/10.1016/0191->  
1564 8141(93)90158-7
- 1565 Shillington, D.J., Scholz, C.A., Chindandali, P.R.N., Gaherty, J.B., Accardo, N.J., Onyango, E.,  
1566 Ebinger, C.J., Nyblade, A.A., 2020. Controls on Rift Faulting in the North Basin of the  
1567 Malawi (Nyasa) Rift, East Africa. *Tectonics* 39, e2019TC005633-e2019TC005633.  
1568 <https://doi.org/10.1029/2019TC005633>
- 1569 Sibson, R.H., 1985. A note on fault reactivation. *Journal of Structural Geology* 7, 751–754.  
1570 [https://doi.org/10.1016/0191-8141\(85\)90150-6](https://doi.org/10.1016/0191-8141(85)90150-6)
- 1571 Sibson, R.H., 1977. Fault rocks and fault mechanisms. *Journal of the Geological Society* 133, 191–  
1572 213. <https://doi.org/10.1144/gsjgs.133.3.0191>
- 1573 Singleton, J.S., Wong, M.S., Johnston, S.M., 2018. the role of calcite-rich metasedimentary  
1574 mylonites in localizing detachment fault strain and influencing the structural evolution of the  
1575 Buckskin-Rawhide metamorphic core complex, west-central Arizona. *Lithosphere* 10, 172–  
1576 193. <https://doi.org/10.1130/L699.1>
- 1577 Skrzypek, E., Schulmann, K., Tabaud, A., Edel, J., 2014. Palaeozoic evolution of the Variscan  
1578 Vosges Mountains. *Geological Society, London, Special Publications* 405, 45–75.  
1579 <https://doi.org/10.1144/SP405.8>
- 1580 Smets, B., Delvaux, D., Ross, K.A., Poppe, S., Kervyn, M., D'Oreye, N., Kervyn, F., 2016. The  
1581 role of inherited crustal structures and magmatism in the development of rift segments:  
1582 Insights from the Kivu basin, western branch of the East African Rift. *Tectonophysics* 683,  
1583 62–76. <https://doi.org/10.1016/j.tecto.2016.06.022>

- 1584 Smith, M., Mosley, P., 1993. Crustal heterogeneity and basement influence on the development of  
1585 the Kenya Rift, East Africa. *Tectonics* 12, 591–606. <https://doi.org/10.1029/92TC01710>
- 1586 Sokoutis, D., Corti, G., Bonini, M., Pierre Brun, J., Cloetingh, S., Mauduit, T., Manetti, P., 2007.  
1587 Modelling the extension of heterogeneous hot lithosphere. *Tectonophysics* 444, 63–79.  
1588 <https://doi.org/10.1016/j.tecto.2007.08.012>
- 1589 Stamps, D.S., Kreemer, C., Fernandes, R., Rajaonarison, T.A., Rambolamanana, G., 2021.  
1590 Redefining East African Rift System kinematics. *Geology* 49, 150–155.  
1591 <https://doi.org/10.1130/G47985.1>
- 1592 Stevens, V.L., Sloan, R.A., Chindandali, P.R., Wedmore, L.N.J., Salomon, G.W., Muir, R.A.,  
1593 2021. The Entire Crust can be Seismogenic: Evidence from Southern Malawi. *Tectonics* 40,  
1594 1–17. <https://doi.org/10.1029/2020TC006654>
- 1595 Styron, R., Pagani, M., 2020. The GEM Global Active Faults Database. *Earthquake Spectra* 36,  
1596 160–180. <https://doi.org/10.1177/8755293020944182>
- 1597 Sykes, L.R., 1978. Intraplate seismicity, reactivation of preexisting zones of weakness, alkaline  
1598 magmatism, and other tectonism postdating continental fragmentation. *Reviews of*  
1599 *Geophysics* 16, 621–688. <https://doi.org/10.1029/RG016i004p00621>
- 1600 Thomas, W.A., 2006. Tectonic inheritance at a continental scale. *GSA Today* 16, 4–11.
- 1601 Tingay, M.R.P., Morley, C.K., Hillis, R.R., Meyer, J., 2010a. Present-day stress orientation in  
1602 Thailand's basins. *Journal of Structural Geology* 32, 235–248.  
1603 <https://doi.org/10.1016/j.jsg.2009.11.008>
- 1604 Tingay, M.R.P., Morley, C.K., Hillis, R.R., Meyer, J., 2010b. Present-day stress orientation in

- 1605 Thailand's basins. *Journal of Structural Geology* 32, 235–248.  
1606 <https://doi.org/10.1016/j.jsg.2009.11.008>
- 1607 Tommasi, A., Knoll, M., Vauchez, A., Signorelli, J.W., Thoraval, C., Logé, R., 2009. Structural  
1608 reactivation in plate tectonics controlled by olivine crystal anisotropy. *Nature Geoscience* 2,  
1609 423–427. <https://doi.org/10.1038/ngeo528>
- 1610 Tommasi, A., Vauchez, A., 2015. Heterogeneity and anisotropy in the lithospheric mantle.  
1611 *Tectonophysics* 661, 11–37. <https://doi.org/10.1016/j.tecto.2015.07.026>
- 1612 Tommasi, A., Vauchez, A., 2001. Continental rifting parallel to ancient collisional belts: an effect  
1613 of the mechanical anisotropy of the lithospheric mantle. *Earth and Planetary Science Letters*  
1614 185, 199–210. [https://doi.org/10.1016/S0012-821X\(00\)00350-2](https://doi.org/10.1016/S0012-821X(00)00350-2)
- 1615 Tron, V., Brun, J.P., 1991. Experiments on oblique rifting in brittle-ductile systems.  
1616 *Tectonophysics* 188, 71–84. [https://doi.org/10.1016/0040-1951\(91\)90315-J](https://doi.org/10.1016/0040-1951(91)90315-J)
- 1617 Twiss, R.J., Unruh, J.R., 1998. Analysis of fault slip inversions: Do they constrain stress or strain  
1618 rate? *Journal of Geophysical Research: Solid Earth* 103, 12205–12222.  
1619 <https://doi.org/10.1029/98JB00612>
- 1620 Upcott, N.M., Mukasa, R.K., Ebinger, C.J., Karner, G.D., 1996. Along-axis segmentation and  
1621 isostasy in the Western rift, East Africa. *Journal of Geophysical Research: Solid Earth* 101,  
1622 3247–3268. <https://doi.org/10.1029/95jb01480>
- 1623 Van Hinsbergen, D.J.J., Buitert, S.J.H., Torsvik, T.H., Gaina, C., Webb, S.J., 2011. The formation  
1624 and evolution of Africa from the Archaean to present: Introduction. *Geological Society*  
1625 *Special Publication* 357, 1–8. <https://doi.org/10.1144/SP357.1>

- 1626 Versfelt, J., Rosendahl, B.R., 1989. Relationships between pre-rift structure and rift architecture  
1627 in Lakes Tanganyika and Malawi, East Africa. *Nature* 337, 354–357.  
1628 <https://doi.org/10.1038/337354a0>
- 1629 Vétel, W., Le Gall, B., Walsh, J.J., 2005. Geometry and growth of an inner rift fault pattern: The  
1630 Kino Sogo Fault Belt, Turkana Rift (North Kenya). *Journal of Structural Geology* 27, 2204–  
1631 2222. <https://doi.org/10.1016/j.jsg.2005.07.003>
- 1632 Vidal, J., Genter, A., 2018. Overview of naturally permeable fractured reservoirs in the central and  
1633 southern Upper Rhine Graben: Insights from geothermal wells. *Geothermics* 74, 57–73.  
1634 <https://doi.org/10.1016/j.geothermics.2018.02.003>
- 1635 Villamor, P., Nicol, A., Seebeck, H., Rowland, J., Townsend, D., Massiot, C., McNamara, D.D.,  
1636 Milicich, S.D., Ries, W., Alcaraz, S., 2017. Tectonic structure and permeability in the Taupō  
1637 Rift: new insights from analysis of LiDAR derived DEMs. *Proceedings 39th New Zealand*  
1638 *Geothermal Workshop*. Rotorua, New Zealand.
- 1639 Walsh, J.J., Nicol, A., Childs, C., 2002. An alternative model for the growth of faults. *Journal of*  
1640 *Structural Geology* 24, 1669–1675. [https://doi.org/10.1016/S0191-8141\(01\)00165-1](https://doi.org/10.1016/S0191-8141(01)00165-1)
- 1641 Wang, D., Wu, Z., Yang, L., Li, W., He, C., 2021. Influence of two-phase extension on the fault  
1642 network and its impact on hydrocarbon migration in the Linnan sag, Bohai Bay Basin, East  
1643 China. *Journal of Structural Geology* 104289. <https://doi.org/10.1016/j.jsg.2021.104289>
- 1644 Wang, K., 2021. If Not Brittle: Ductile, Plastic, or Viscous? *Seismological Research Letters*.  
1645 <https://doi.org/10.1785/0220200242>
- 1646 Wedmore, L.N.J., Biggs, J., Floyd, M., Fagereng, Mdala, H., Chindandali, P., Williams, J.N.,

- 1647 Mphepo, F., 2021. Geodetic Constraints on Cratonic Microplates and Broad Strain During  
1648 Rifting of Thick Southern African Lithosphere. *Geophysical Research Letters* 48.  
1649 <https://doi.org/10.1029/2021GL093785>
- 1650 Wedmore, L.N.J., Biggs, J., Williams, J.N., Fagereng, Dulanya, Z., Mphepo, F., Mdala, H., 2020a.  
1651 Active Fault Scarps in Southern Malawi and Their Implications for the Distribution of Strain  
1652 in Incipient Continental Rifts. *Tectonics* 39. <https://doi.org/10.1029/2019TC005834>
- 1653 Wedmore, L.N.J., Williams, J.N., Biggs, J., Fagereng, Å., Mphepo, F., Dulanya, Z., Willoughby,  
1654 J., Mdala, H., Adams, B.A., 2020b. Structural inheritance and border fault reactivation during  
1655 active early-stage rifting along the Thyolo fault, Malawi. *Journal of Structural Geology* 139,  
1656 104097. <https://doi.org/10.1016/j.jsg.2020.104097>
- 1657 Wheeler, W.H., Karson, J.A., 1989. Structure and kinematics of the Livingstone Mountains border  
1658 fault zone, Nyasa (Malawi) Rift, southwestern Tanzania. *Journal of African Earth Sciences*  
1659 (and the Middle East) 8, 393–413. [https://doi.org/10.1016/S0899-5362\(89\)80034-X](https://doi.org/10.1016/S0899-5362(89)80034-X)
- 1660 Whipp, P.S., Jackson, C.A.L., Gawthorpe, R.L., Dreyer, T., Quinn, D., 2014. Normal fault array  
1661 evolution above a reactivated rift fabric; a subsurface example from the northern Horda  
1662 Platform, Norwegian North Sea. *Basin Research* 26, 523–549.  
1663 <https://doi.org/10.1111/br.12050>
- 1664 Wijns, C., Weinberg, R., Gessner, K., Moresi, L., 2005. Mode of crustal extension determined by  
1665 rheological layering. *Earth and Planetary Science Letters* 236, 120–134.  
1666 <https://doi.org/10.1016/j.epsl.2005.05.030>
- 1667 Williams, J.N., Fagereng, Å., Wedmore, L.N.J., Biggs, J., Mdala, H., Mphepo, F., Hodge, M.,  
1668 2022. Low Dissipation of Earthquake Energy Where a Fault Follows Pre-Existing

- 1669 Weaknesses: Field and Microstructural Observations of Malawi's Bilila-Mtakataka Fault.  
1670 Geophysical Research Letters 49, 1–11. <https://doi.org/10.1029/2021GL095286>
- 1671 Williams, J.N., Fagereng, Å., Wedmore, L.N.J., Biggs, J., Mphepo, F., Dulanya, Z., Mdala, H.,  
1672 Blenkinsop, T., 2019. How Do Variably Striking Faults Reactivate During Rifting? Insights  
1673 From Southern Malawi. *Geochemistry, Geophysics, Geosystems* 20, 3588–3607.  
1674 <https://doi.org/10.1029/2019GC008219>
- 1675 Williams, J.N., Mdala, H., Fagereng, Å., Wedmore, L.N.J., Biggs, J., Dulanya, Z., Chindandali,  
1676 P., Mphepo, F., 2021. A systems-based approach to parameterise seismic hazard in regions  
1677 with little historical or instrumental seismicity: active fault and seismogenic source databases  
1678 for southern Malawi. *Solid Earth* 12, 187–217. <https://doi.org/10.5194/se-12-187-2021>
- 1679 Wilson, J.T., 1966. Did the Atlantic Close and then Re-open? *Nature* 211, 676–681.
- 1680 Wilson, R.W., Holdsworth, R.E., Wild, L.E., McCaffrey, K.J.W., England, R.W., Imber, J.,  
1681 Strachan, R.A., 2010. Basement-influenced rifting and basin development: a reappraisal of  
1682 post-Caledonian faulting patterns from the North Coast Transfer Zone, Scotland. *Geological*  
1683 *Society, London, Special Publications* 335, 795–826. <https://doi.org/10.1144/SP335.32>
- 1684 Yale, D.P., 2003. Fault and stress magnitude controls on variations in the orientation of in situ  
1685 stress. *Geological Society Special Publication* 209, 55–64.  
1686 <https://doi.org/10.1144/GSL.SP.2003.209.01.06>
- 1687 Yardley, B., Gleeson, S., Bruce, S., Banks, D., 2000. Origin of retrograde fluids in metamorphic  
1688 rocks. *Journal of Geochemical Exploration* 69, 281–285. <https://doi.org/10.1016/S0375->  
1689 [6742\(00\)00132-1](https://doi.org/10.1016/S0375-6742(00)00132-1)

- 1690 Yeomans, C.M., Shail, R.K., Eyre, M., 2020. The importance of tectonic inheritance and  
1691 reactivation in geothermal energy exploration for EGS resources in SW England. Proceedings  
1692 World Geothermal Congress 2020. Reykjavik, Iceland.
- 1693 Zang, A., Stephansson, O., 2010. Stress Field of the Earth's Crust, 1st ed. Springer Netherlands.  
1694 <https://doi.org/10.1007/978-1-4020-8444-7>
- 1695 Zhang, J.J., 2019. Abnormal pore pressure mechanisms. *Applied Petroleum Geomechanics*.  
1696 Elsevier, 233–280. <https://doi.org/10.1016/B978-0-12-814814-3.00007-1>
- 1697 Zhang, Y.-Z., Dusseault, M.B., Yassir, N.A., 1994. Effects of rock anisotropy and heterogeneity  
1698 on stress distributions at selected sites in North America. *Engineering Geology* 37, 181–197.  
1699 [https://doi.org/10.1016/0013-7952\(94\)90055-8](https://doi.org/10.1016/0013-7952(94)90055-8)
- 1700 Zwaan, F., Chenin, P., Erratt, D., Manatschal, G., Schreurs, G., 2021a. Complex rift patterns, a  
1701 result of interacting crustal and mantle weaknesses, or multiphase rifting? Insights from  
1702 analogue models. *Solid Earth* 12, 1473–1495. <https://doi.org/10.5194/se-12-1473-2021>
- 1703 Zwaan, F., Chenin, P., Erratt, D., Manatschal, G., Schreurs, G., 2021b. Competition between 3D  
1704 structural inheritance and kinematics during rifting: Insights from analogue models. *Basin*  
1705 *Research* 1–31. <https://doi.org/10.1111/bre.12642>
- 1706 Zwaan, F., Schreurs, G., 2020. Rift segment interaction in orthogonal and rotational extension  
1707 experiments: Implications for the large-scale development of rift systems. *Journal of*  
1708 *Structural Geology* 140, 104119. <https://doi.org/10.1016/j.jsg.2020.104119>
- 1709 Zwaan, F., Schreurs, G., 2017. How oblique extension and structural inheritance influence rift  
1710 segment interaction: Insights from 4D analog models. *Interpretation* 5, SD119–SD138.

1711 <https://doi.org/10.1190/INT-2016-0063.1>

1712 Zwaan, F., Schreurs, G., Naliboff, J., Buitter, S.J.H., 2016. Insights into the effects of oblique  
1713 extension on continental rift interaction from 3D analogue and numerical models.  
1714 *Tectonophysics* 693, 239–260. <https://doi.org/10.1016/j.tecto.2016.02.036>

1715